12

Predictability of seasonal climate variations: a pedagogical review

J. Shukla, J. L. Kinter III
Center for Ocean–Land–Atmosphere Studies, Calverton, Maryland

12.1 Introduction

It is well known that the day-to-day changes in the large-scale atmospheric circulation are not predictable beyond two weeks. The small-scale rainfall patterns associated with the large-scale circulation patterns may not be predictable beyond even a few days. However, the space–time averages of certain atmospheric and oceanic variables are predictable for months to seasons. This chapter gives a pedagogical review of the ideas and the results that have led to our current understanding and the status of the predictability of seasonal climate variations.

We first review the current status of the understanding of the limits of the predictability of weather. We adopt Lorenz' classical definition of the predictability of weather as the range at which the difference between forecasts from two nearly identical initial conditions is as large in a statistical sense as the difference between two randomly chosen atmospheric states. With this definition of predictability, it is implied that the upper limit of predictability depends on the saturation value of the maximum possible error, which, in turn, is determined by the climatological variance. Lorenz provided a simple conceptual model in which the upper limit of weather prediction skill is described by three fundamental quantities: the size of the initial error, the growth rate of the error and the saturation value of the error. This simple model is able to explain the current status of the seasonal, regional and hemispheric variations of numerical weather prediction (NWP) skill. For example, winter is more

Predictability of Weather and Climate, ed. Tim Palmer and Renate Hagedorn. Published by Cambridge University Press.

predictable than summer, and the midlatitudes are more predictable than the tropics, simply because the saturation value of forecast error is much larger in winter and in the midlatitudes than in the tropics. The progress of NWP skill for the medium range over the past 25 years can be explained almost entirely by the reduction in the forecast error at day one, which, in turn, can be explained by the reduction in the initial error. The models and data assimilation techniques have steadily improved, thereby decreasing the initial error by 50%, while the growth rate of initial error has increased only modestly, resulting in steady improvement in the skill of NWP models for days 2–10.

We then will show that, in spite of the two-week upper limit of deterministic weather predictability, the effects of anomalous boundary conditions at the Earth's surface (sea surface temperature, snow, soil moisture, etc.) are sufficiently large to produce statistically significant anomalies in the seasonal mean atmospheric circulation. It is found, somewhat paradoxically, that the anomalous surface boundary conditions are much more influential in the tropics, where the deterministic limit of weather predictability is relatively short, than in midlatitudes, where the limit of weather predictability is relatively long. We review some atmospheric general circulation model (GCM) experiments which have helped advance our understanding of the boundary-forced predictability.

We then address the question of the predictability of the boundary conditions themselves. Since anomalous boundary conditions are produced by interactions between the ocean, atmosphere and land-surface processes, we review the status of the predictability of seasonal mean climate anomalies using coupled ocean–atmosphere–land models. We also address the question of seasonal predictability in a changing climate.

12.2 Predictability of weather

In a series of three papers that appeared in the late 1960s, E. Lorenz laid the theoretical groundwork for weather predictability that has been used in the subsequent decades to great advantage. In a comprehensive study of the predictability of the 28-variable model (Lorenz, 1965), in which for the first time he calculated the singular vectors, he showed that error growth is a strong function of the structure of the initial atmospheric flow and he estimated the doubling time of synoptic-scale errors to be a few days. He then employed a turbulence model (Lorenz, 1969a), assuming a $-5/3$ power law for the energy density spectrum, to compute the error saturation time, defined as the time at which the error energy at a given wave number becomes equal to the energy at that wave number prescribed in the initial conditions. He showed that scale interactions cause the error in the smallest scales to saturate the fastest, producing errors at synoptic scales within a few days after the initial time. Lorenz also devised a method for estimating the predictability of the atmosphere by searching for

analogues or states that are sufficiently close in some phase space to permit using the evolution of the distance between the analogous states as a proxy for error growth in the classical predictability sense (Lorenz, 1969b). He found that the observational record available at that time was insufficient to find analogues that could be used in this way; nevertheless, he assumed a quadratic model for the error growth to estimate that the doubling time of small errors would be 2.5 days. These studies, along with several others that examined the characteristics of turbulent flows (Leith, 1971; Leith and Kraichnan, 1972) and later attempts to refine the predictability estimates with analogues (Gutzler and Shukla, 1984) and atmospheric GCMs (Smagorinsky, 1963; Charney *et al.*, 1966; Williamson and Kasahara, 1971; Lorenz, 1982; Simmons *et al.*, 1995; see Shukla, 1985 for a review) have shown that the predictability of weather is characterised completely by the growth rate and saturation value of small errors. While early atmospheric GCM estimates of error doubling time were relatively different (e.g. Charney, 1966), the diverse techniques to estimate the doubling time have converged to become remarkably consistent, all around two days. The most recent estimate available from ECMWF is 1.5 days (Simmons and Hollingsworth, 2002).

The ECMWF has shown recently that, as suggested by Lorenz (1982), the reduction in the error at day 1 has led to improvements in skill after 10 days. The expectation that the reduction in error might be overwhelmed by the increase in growth rate (smaller errors grow faster in the Lorenz model) has not occurred. A combination of improvements in the atmospheric GCM and better assimilation of available observations has led to a sustained reduction in error through at least day 7 of the forecast.

12.3 Predictability of seasonal averages – from weather prediction to seasonal prediction

One implication of the fact that the predictability of weather is a function of the error growth rate and saturation value is that predictability is quite different in the tropics and the extratropics. In the tropics, the variance of daily fluctuations, and hence the saturation value of errors, is much smaller than it is in the extratropics (Shukla, 1981a). Similarly, the error growth rate in the tropics, dominated as it is by instabilities associated with convection, is larger than in the extratropics where the error growth is primarily associated with baroclinic instability. Based on these considerations, Shukla (1981a) showed that the upper limit of deterministic predictability in the tropics is shorter than in the extratropics. By contrast, the short-term climate fluctuations in the tropics are dominated by the slowly varying boundary conditions, as will be described below, so, ironically, the seasonal means in the tropics are more predictable than the extratropics, in contrast to the situation for weather predictability.

Predictability also varies with spatial scale of motion. Several studies (Smagorinsky, 1969; Shukla, 1981b) have shown that the long waves are more predictable than

the short waves in the extratropics. This is primarily due to the larger saturation value of error for the long waves, which in general have larger amplitude than the short waves. This is also consistent with the long-standing view of synoptic forecasters who have relied on systematic progressions of large-scale patterns in the atmosphere, variously called *Grosswetterlagen*, weather regimes, or centres of action (Hess and Brezowsky, 1969; Namias, 1986; Barnston and Livezey, 1987).

The main determinant of seasonal atmospheric predictability is the slowly varying boundary conditions at the Earth's surface (Charney and Shukla, 1977; Lorenz, 1979; Shukla, 1981b). It is well known that the lower boundary conditions of the Earth's atmosphere vary more slowly than the day-to-day variations of the weather and that, insofar as the boundary conditions can influence the large-scale atmospheric circulation, the time and space averages of the atmosphere are predictable at timescales beyond the upper limit of instantaneous predictability of weather. The surface boundary conditions include the sea surface temperature (SST), which governs the convergence of moisture flux as well as the sensible and latent heat fluxes between the ocean and atmosphere; the soil moisture, which alters the heat capacity of the land surface and governs the latent heat flux between continents and the atmosphere; vegetation, which regulates surface temperature as well as the latent heat flux to the atmosphere from land surfaces; snow, which participates in the surface radiative balance through its effect on surface albedo and in the latent heat flux, introducing a lag due to the storage of water in solid form in winter which is melted or evaporated in the spring and changes the soil wetness; and sea ice, which likewise participates in the energy balance and inhibits latent heat flux from the ocean. In each of these boundary conditions, anomalies can influence the surface fluxes and low-level atmospheric convergence through changes in the horizontal temperature and pressure gradients, at times leading to three-dimensional atmospheric heating anomalies, which in turn affect the entire atmospheric circulation.

12.3.1 Oceanic influences

Over the past 20 years, literally hundreds of numerical experiments have been conducted to test the hypothesis that the lower boundary conditions affect the seasonal circulation. Sensitivity studies have examined the effects of SST and sea ice anomalies in the tropical Pacific (e.g. Shukla and Wallace, 1983; Fennessy *et al.*, 1985), the tropical Atlantic (e.g. Moura and Shukla, 1981), the Arabian Sea (Shukla, 1975; Shukla and Misra, 1977), the north Pacific Ocean (Namias, 1969; Alexander and Deser, 1995), the north Atlantic Ocean (Palmer and Sun, 1985; Bhatt *et al.*, 1998), global SST anomalies (e.g. Miyakoda *et al.*, 1983; Kinter *et al.*, 1988; Shukla and Fennessy, 1988; Shukla *et al.*, 2000a, 2000b), sea ice (e.g. Randall *et al.*, 1998), mountains (Hahn and Manabe, 1975; Wallace *et al.*, 1983), deforestation (e.g. Nobre *et al.*, 1991), surface albedo anomalies associated with desertification (Charney, 1975; Xue and Shukla, 1993; Dirmeyer and Shukla, 1996), surface roughness anomalies (Sud

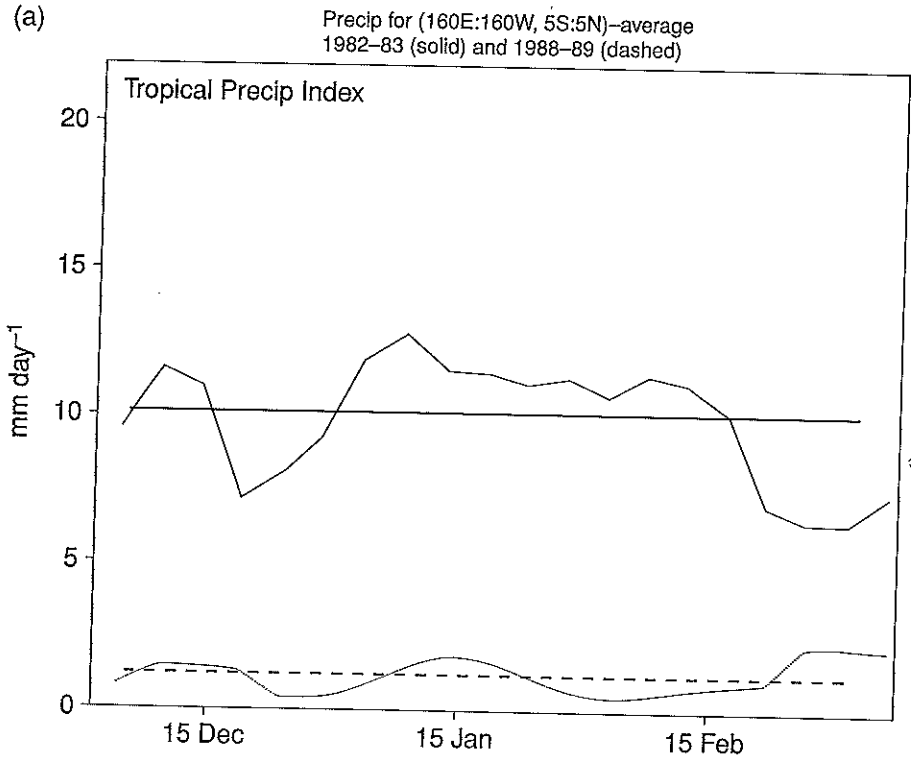

Figure 12.1 Effects of SST anomalies on tropical precipitation and extratropical atmospheric circulation. (a) and (b) show precipitation area-averaged over (160° E–160° W, 5° S–5° N), for the boreal winter season. (c) and (d) show the difference between two area-averages of the extratropical 500 hPa geopotential height: (120° W–110° W, 50° N–60° N) minus (170° W–160° W, 40° N–50° N). Anomalously warm tropical Pacific SST years are shown as a solid curve (1982–83 in a and c and 1986–87 in b and d), and anomalously cold tropical Pacific SST years are shown as dashed curves (1988–89 in a and c and 1984–85 b and d). The thick horizontal lines are the seasonal averages of the two time series.

et al., 1988), soil wetness anomalies (e.g. Dirmeyer and Shukla, 1993; Fennessy and Shukla, 1999), vegetation (Dickinson, 1984; Sellers *et al.*, 1986), and snow cover (e.g. Hahn and Shukla, 1976; Barnett *et al.*, 1988; Cohen and Rind, 1991; Bamzai and Marx, 2000). The result of all these experiments is that, under favourable conditions of the large-scale flow, and for certain structure, magnitude and location of the boundary anomalies, there is substantial evidence that the seasonal variations of the tropical climate are predictable and there is some possibility of predicting the extratropical climate as well (Palmer and Shukla, 2000).

The dependence of the predictability of the climate on location and season is illustrated in Figures 12.1–12.3. Parts (a) and (b) of Figure 12.1 show an index of tropical climate variability for the boreal winter season. Two years, shown as a solid curve, have boundary forcing, i.e. SST in the tropical Pacific, that is significantly warmer

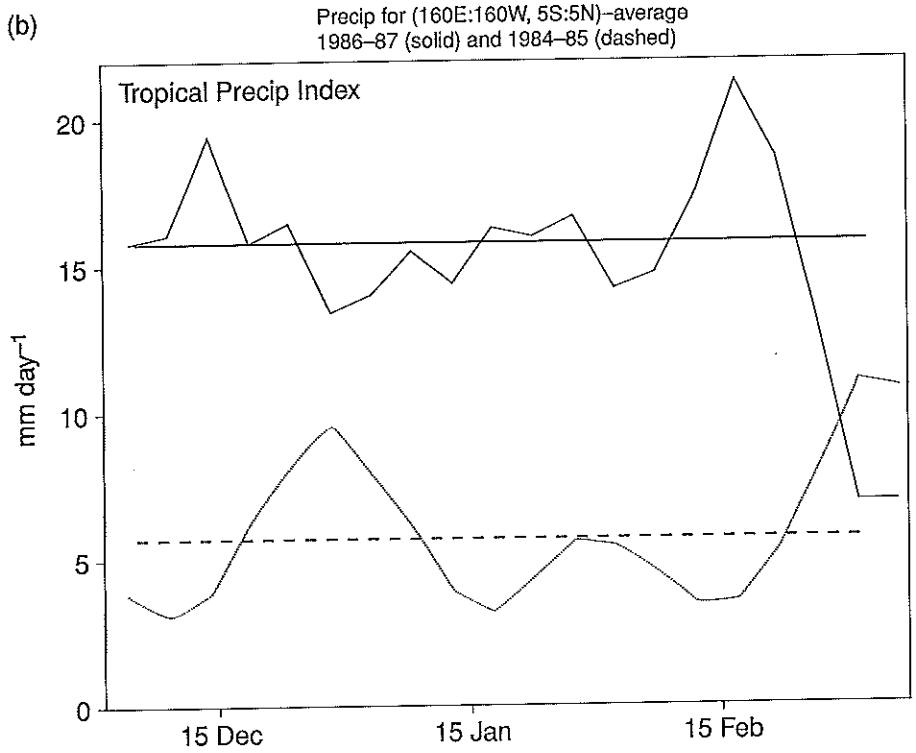

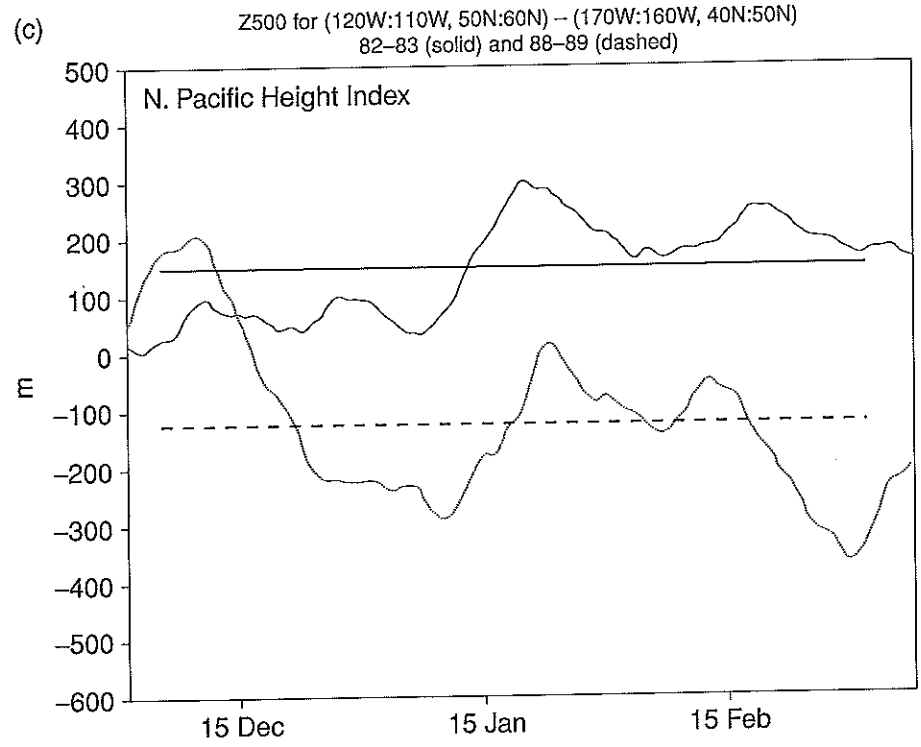

Figure 12.1 (*cont.*)

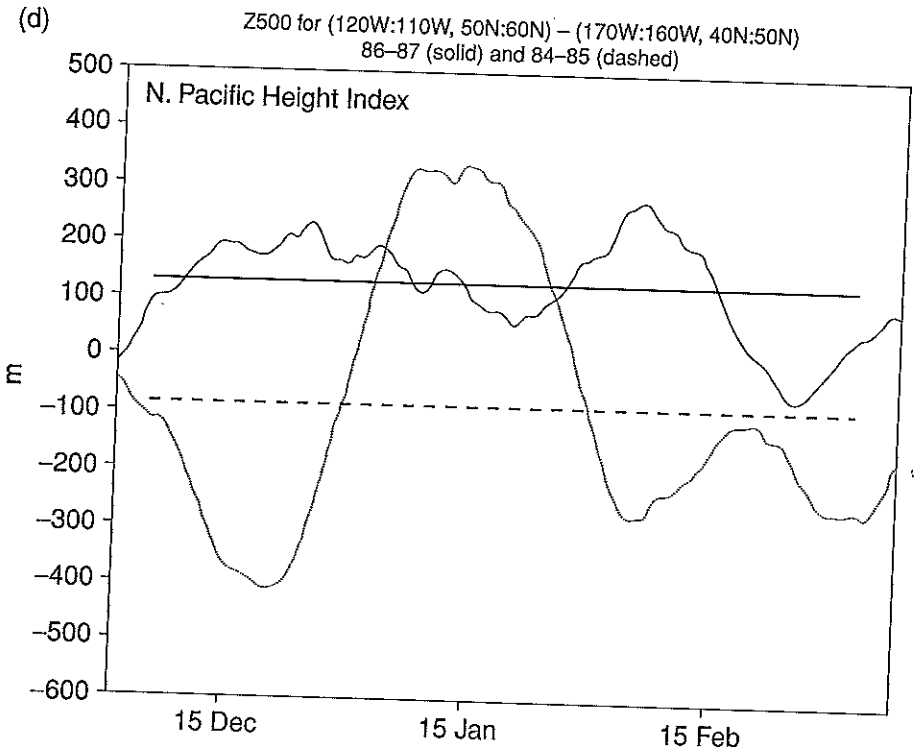

Figure 12.1 (*cont.*)

than usual. Two other years, shown as a dotted curve, have tropical Pacific SST that is significantly cooler than usual. In Figure 12.1 (c, d), an index of extratropical climate variability in boreal winter is shown for the same years. In the extratropical winter, the seasonal means of the two years are separated by a statistically significant amount that is *comparable to* the magnitude of the intraseasonal variation. In the tropics, the seasonal means are separated by a statistically significant amount that is *much larger than* the magnitude of intraseasonal variations. The variance of a typical quantity like sea-level pressure in the extratropical winter is larger than in the tropics. The boundary-forced seasonal mean differences in the tropics are relatively large. As shown schematically in Figure 12.2, the typical spread of forecasts initialised with slightly perturbed initial conditions becomes saturated at about five days or less in the tropics (dashed line) and about 10 days in the extratropics. Figure 12.3 illustrates the large difference in day-to-day variability between the tropics (typical values of 4 m/s) and the extratropics (typical values of 10 m/s).

An anomaly in the boundary conditions can affect the seasonal mean, large-scale atmospheric circulation through a relatively complex pathway, which is illustrated schematically in Figure 12.4. An SST anomaly, for example, locally alters the sensible and latent heat fluxes from ocean to atmosphere, thereby changing the temperature

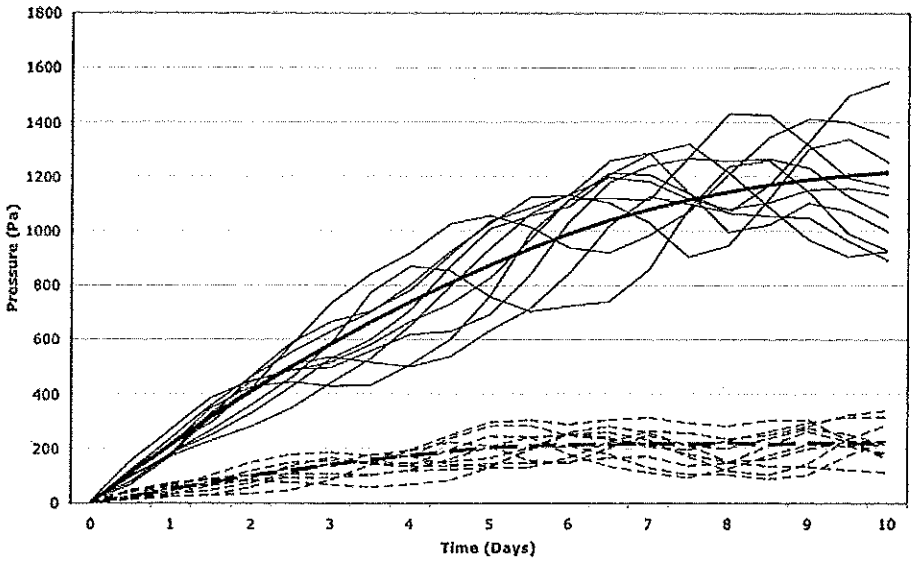

Figure 12.2 Schematic diagram illustrating the error growth in the tropics (dashed) and the extratropics (solid). Both thick lines depict the rates at which initially different states reach the boundary-forced state. The thin lines show typical spread of forecasts initialised with slightly perturbed initial conditions on day 0.

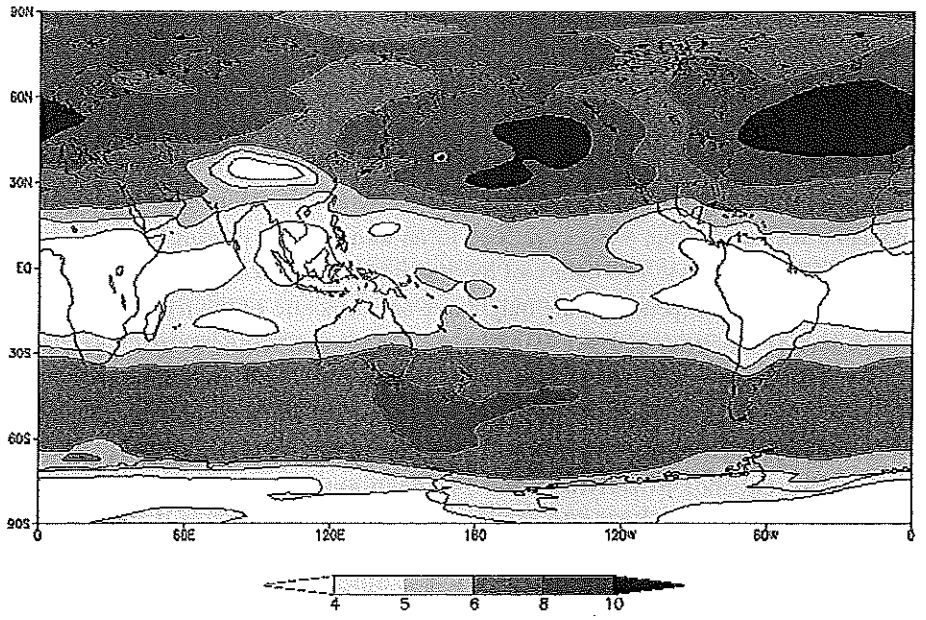

Figure 12.3 Standard deviation of daily values of 500 hPa zonal wind, computed with respect to individual monthly means for December, January and February, averaged over 1970–1999 (m/s).

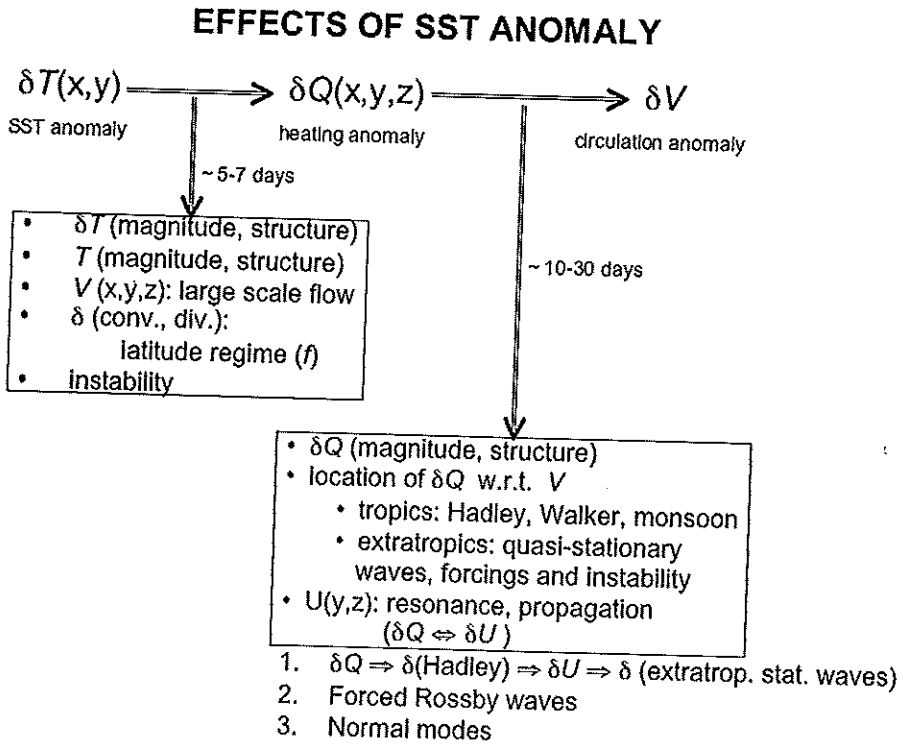

Figure 12.4 Schematic diagram of the effects of boundary condition anomalies on large-scale atmospheric heating and large-scale atmospheric circulation. See text for explanation.

and humidity in the atmosphere nearest the surface. Depending on the scale and magnitude of the SST anomaly, such changes can be relatively unimportant for the seasonal mean, or they can alter the static stability and moisture flux convergence available for convection, which can lead to an atmospheric heating anomaly over the course of 5–7 days. The nature of the heating anomaly associated with a given SST anomaly also depends on the magnitude and structure of the background SST on which it is superimposed. For example, a large warm SST anomaly that is superimposed on a very cold background ocean temperature will have little effect and likely will not lead to a large-scale atmospheric heating anomaly. The development of an atmospheric heating anomaly also depends on the structure of the large-scale atmospheric circulation overlying the SST anomaly as well as the degree to which the convergence and divergence of the atmospheric circulation are affected. A given SST anomaly may significantly alter the surface temperature gradient and, consequently, the surface pressure gradient, which then changes the low-level atmospheric convergence. The latter depends on the latitude of the anomaly, because the further the location is from the equator the less significant the divergent circulation associated with the pressure gradient anomalies is with respect to the rotational component of the flow. Changes in the divergent flow directly affect the moisture flux convergence

(especially in the tropics), which is important in driving convection, thereby altering the deep heating of the atmosphere through latent heat release. Under the right conditions, a positive feedback loop involving boundary layer moisture flux convergence, precipitation and deep tropospheric heating, can significantly alter the large-scale atmospheric circulation.

Once a three-dimensional atmospheric heating anomaly has developed, it can influence the large-scale atmospheric circulation over the course of 10 to 30 days. Again, this is dependent on the size, magnitude and structure of the heating anomaly as well as several other factors. For example, if the heating anomaly is located in the tropics, its effect on the circulation depends on its position relative to the rising and descending branches of the Hadley and Walker circulations. Associated with the large land masses and the air–sea contrast in the tropics, the seasonal monsoon is the largest feature of the large-scale circulation, so the location of a heating anomaly with respect to the centres of the monsoon circulations is also an important factor. In the extratropics, matters are more complex, because there is a non-linear dynamic interaction between the zonal mean flow, the quasi-stationary eddies and the transient eddies. Similar heating anomalies located on different sides of a jet or at different phases of a stationary wave will have dramatically different effects, either through the forcing of transient waves or through an alteration of the mean flow by means of instability or wave–mean flow interaction. The effects of a given heating anomaly may be non-local as well. For example, a heating anomaly in the tropics may lead to a change in the Hadley circulation, which can thereby alter the zonal mean flow in the subtropics or mid-latitudes and change the orographically forced response. That change in the mean circulation can also, in turn, lead to an altered index of refraction for dispersive planetary waves. Through resonance, the forced waves might feed back on the tropical circulation and change the heating anomaly itself. There is also a possibility of teleconnections through propagation and dispersion of Rossby waves or through normal mode-type responses to forcing.

The role of boundary conditions in enhancing the predictability of time averages was demonstrated by Shukla (1998) through a set of numerical experiments with the COLA atmospheric GCM. Two sets of five-member ensemble simulations were conducted with very different initial conditions but identical observed SST specified as lower boundary conditions. The initial conditions were for December 1982 and December 1988, which corresponded to La Niña and El Niño years, and therefore had very different tropical atmospheric states. It was found that, in spite of very large differences in the initial conditions but the same (observed) SST for 1982–3, the simulated tropical winter mean precipitation pattern was nearly identical and had great similarity to the observed precipitation anomaly. Likewise, for the winter of 1988–9, the two simulations with very different initial states were also nearly identical, and were very similar to the observed precipitation anomaly for that year. An examination of the day-by-day simulation of tropical Pacific rainfall and circulation showed that the simulations with two very different initial conditions began to converge under the influence of the boundary conditions, and they became statistically indistinguishable

within 7–10 days. This experiment confirmed what had been suspected for quite some time, namely that some parts of the tropics are so strongly forced by the underlying SST anomaly that even a very large perturbation in the initial conditions does not change the simulation of the seasonal mean rainfall.

In the same experiments, it was also found that even the extratropical seasonal mean circulation anomalies, especially over the Pacific–North American region, were largely determined by the SST anomalies. For example, the 500 hPa seasonal mean height anomalies for two very different initial conditions were nearly identical for a given SST anomaly. This suggests that the high predictability of the tropical atmosphere can also enhance the predictability of the extratropical atmosphere if the SST boundary forcing is quite strong. There has been some debate among the researchers whether boundary forcing merely changes the frequency of midlatitude modes of variability, or whether the boundary-forced variability is distinctly different from the unforced variability (Straus and Shukla, 2000).

One dramatic example of the fact, that, in spite of the high degree of variability in the extratropical atmosphere, tropical forcing can produce predictable effects in the extratropics, is shown in Figure 12.5 (colour plate). The bottom panel of the figure shows the difference in the boreal winter 500 hPa geopotential height field between large positive tropical Pacific SST anomaly (El Niño) years (1983, 1987 and 1992) and large negative (La Niña) years (1985 and 1989). The top panel shows an ensemble-mean simulation of the same field produced by an atmospheric GCM forced by the observed SST in those years. The ensemble average of several runs started from slightly different initial states was computed to filter the unpredictable component of the simulations. There is an uncanny match in both phase and amplitude of the simulated difference to the observed difference (anomaly correlation coefficient = 0.98 for the spatial domain shown in the figure).

This result has been reproduced by several atmospheric GCMs. Figure 12.6 shows the anomaly correlation coefficient for each of three different models (COLA, NSIPP and NCEP atmospheric GCMs) in each of 18 years. The years have been reordered in ascending absolute values of the corresponding NINO3 index, an indicator of the amplitude of the tropical Pacific SST anomaly, to show that the predictability of the extratropical Pacific–North American regional height anomalies depends on the magnitude of the forcing. A systematic evaluation of the possibility of dynamical seasonal prediction has been made (Shukla *et al.*, 2000a, 2000b)

It is by no means a given, however, that seasonal predictions, even in the presence of relatively strong SST anomalies in the tropical Pacific, will be highly skilful for all quantities and in all cases. As an example, a pair of seasonal hindcasts, produced using one of the models whose skill scores are shown in Figure 12.6, is shown in Figure 12.7 for two La Niña cases, 1989 and 1999. In both cases, the tropical Pacific SST forcing is fairly strong. The surface air temperature anomaly hindcast is quite good, both in terms of geographical distribution and amplitude, for the 1989 case, but only somewhat resembles the observed in the 1999 case. This is indicative of some of the difficulties

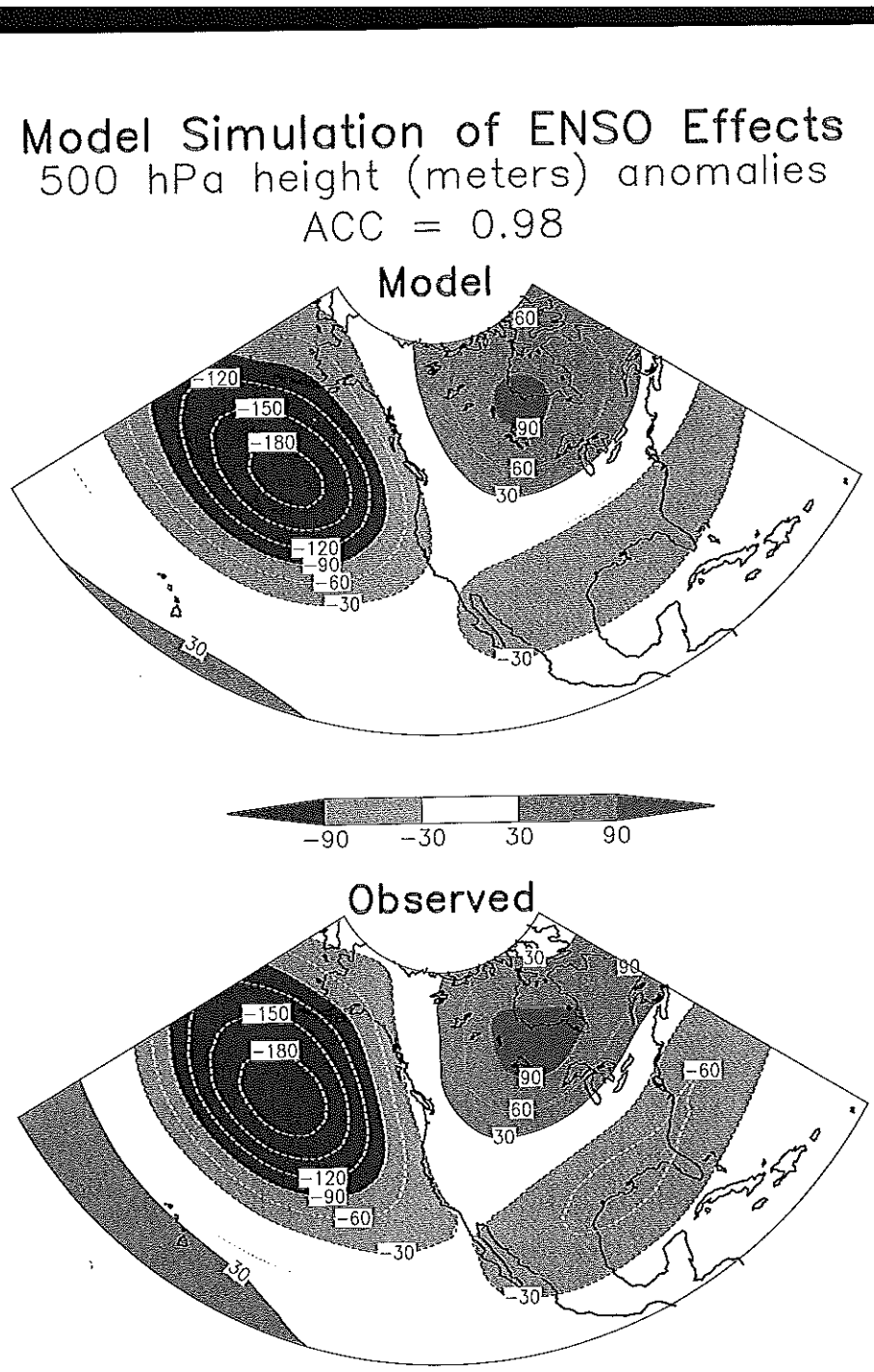

Figure 12.5 (See also colour plate section.) Composite, ensemble-mean AGCM simulation of January–February–March seasonal mean difference of 500 hPa geopotential height. Average of three years with warm SST anomalies in the eastern tropical Pacific (1983, 1987 and 1992) minus average of two years with cold SST anomalies (1985 and 1989). The ensemble of 10 model simulations were made with observed SST specified as lower boundary conditions and slightly different initial conditions in each ensemble member. The model used is the COLA atmospheric GCM.

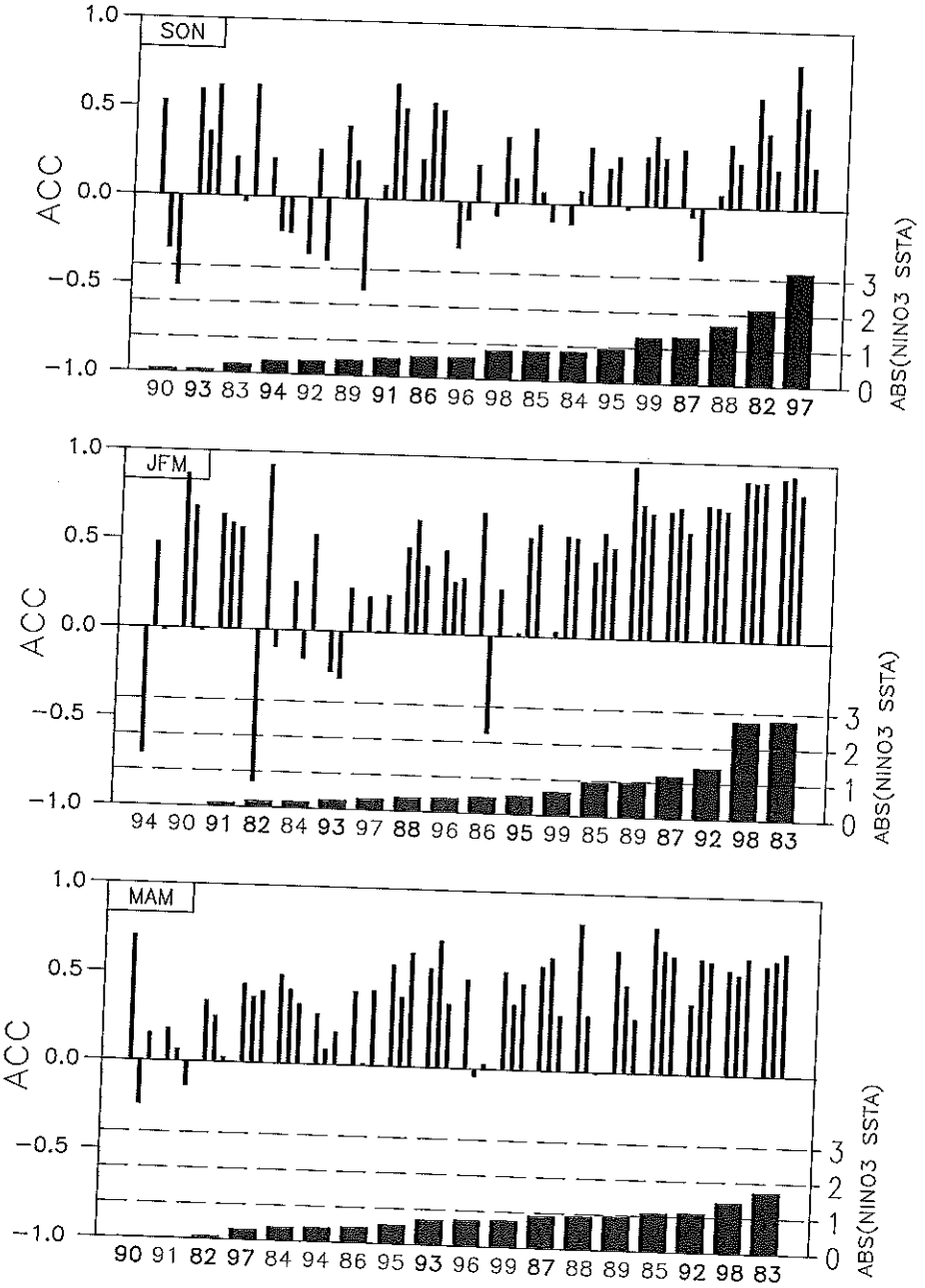

Figure 12.6 Each thin vertical bar shows the pattern correlation of the ensemble-mean seasonal mean 200-hPa height of an atmospheric GCM with the observed seasonal mean over North America 15°–70° N and 180°–60° W. The pattern correlation is computed separately for each year and for each GCM; the bars show the results for the COLA, NSIPP, and NCEP GCMs from left to right. The years are ordered by the absolute value of the NINO-3 index, increasing to the right and shown by the thick vertical bars. Bold and light numbers indicate warm and cold years respectively. Results (top) for boreal autumn (Sep–Nov), (middle) for boreal winter (Jan–Mar), and (bottom) for boreal spring (Mar–May).

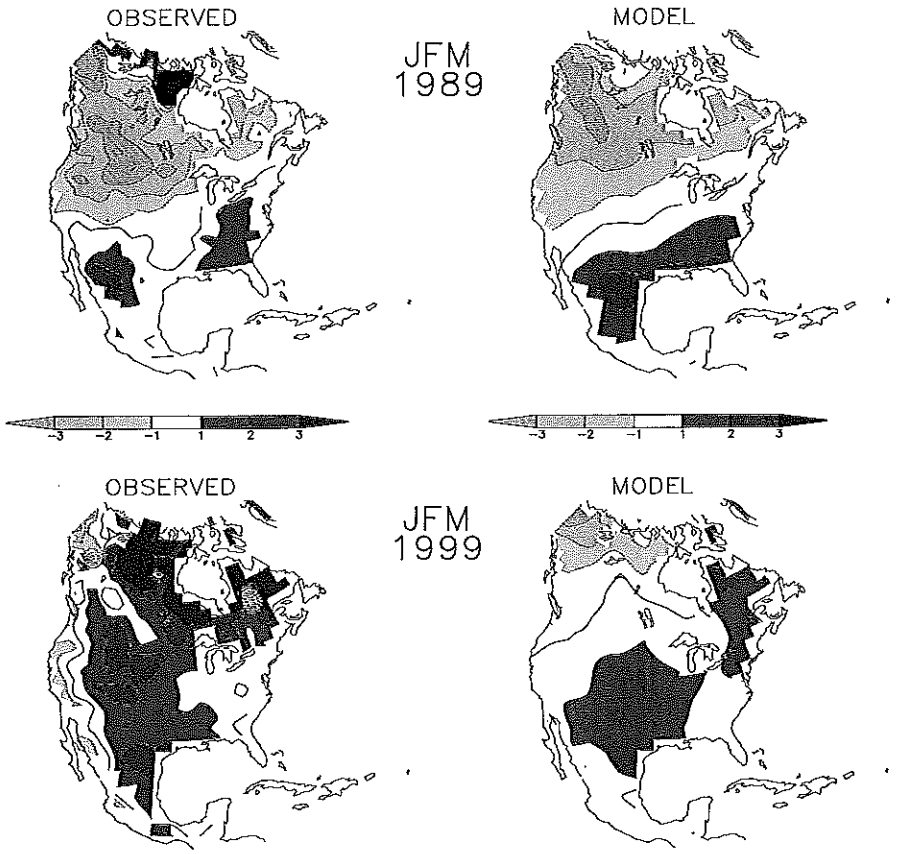

Figure 12.7 The seasonal mean surface air temperature anomaly for January–March 1989 (top row) and January–March 1999 (bottom row) from the observed (left column) and from a simulation in which the observed SST and sea ice were specified as the lower boundary conditions of an atmospheric GCM.

of translating the advances in understanding predictability into real improvements in seasonal prediction.

Likewise there is an asymmetry between warm and cold ENSO events in the extratropical variability associated with each. In particular, the warm and cold events influence the internal variability in the Pacific–North America region. Figure 12.8, comparing the ratio of interensemble variance computed for three different atmospheric GCMs, shows that all the models have more variability in cold events than in warm events, and, for some parts of the region (near the Aleutian Islands, over the west coast and south-eastern USA), the cold event variance exceeds the warm event variance by a factor of two or more.

12.3.2 Land influences

The physical processes at the land surface have effects on the climate, including the components of the hydrologic cycle and the atmospheric circulation, on a wide range

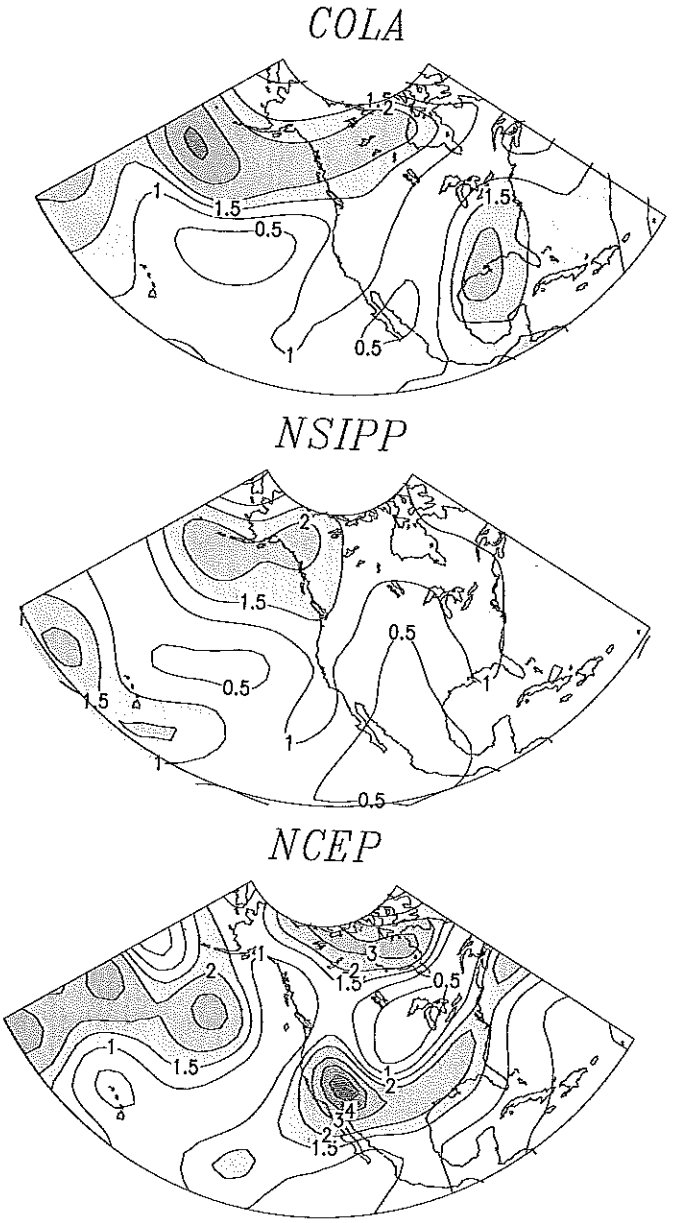

Figure 12.8 Ratio of the January–March mean intraensemble variance of Φ200 between cases with cold tropical Pacific SST (1985 and 1989) and cases with warm tropical Pacific SST (1983, 1987, 1992, and 1995).

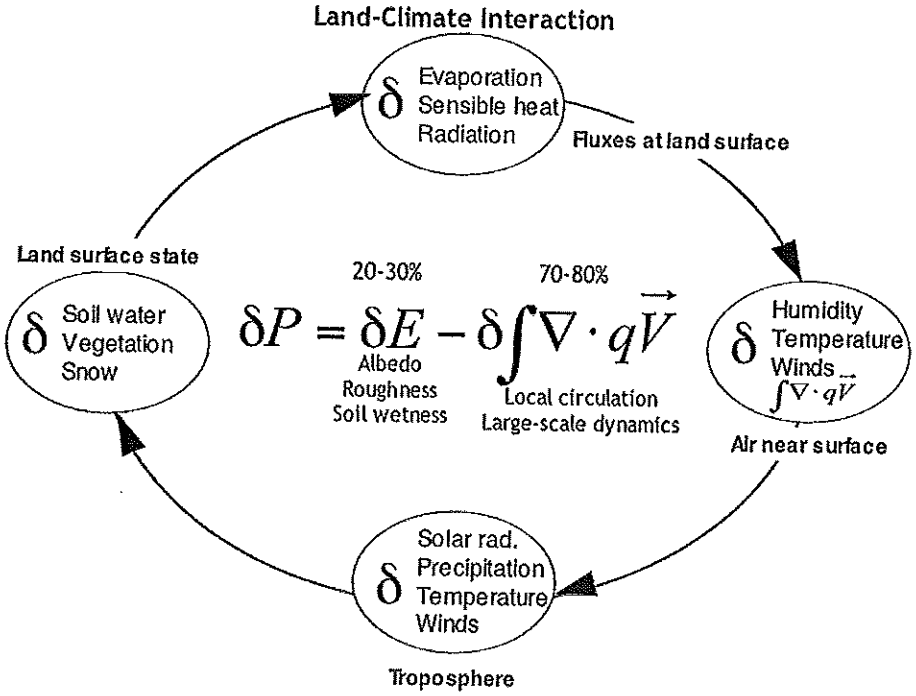

Figure 12.9 Schematic diagram showing the cycle of interactions between the land surface and the climate. Beginning with the oval at the left, a change in the land surface state (soil wetness, vegetation or snow) leads to a change in the fluxes of water, heat and radiation between the land surface and the atmosphere (oval at top). These changes can, in turn, lead to changes in the humidity and temperature of the air near the surface, as well as changes in the wind due to changes in the gradients of surface temperature or pressure (oval at right). The changes occurring near the surface can produce changes throughout the atmospheric column that occur in solar radiative flux (cloudiness), precipitation, air temperature and winds (oval at bottom). These changes can then affect the land surface state, completing the feedback loop.

of temporal and spatial scales (e.g. Dirmeyer and Shukla, 1993). The properties of the land surface, such as soil wetness, snow cover, and vegetation, affect both the evolution and predictability of climate (Dickinson, 1984). For example, soil moisture determines the rate of evapotranspiration as well as the partitioning of incoming radiation into sensible and latent heat flux. Likewise, the spatial distribution and temporal variability of vegetation, soil wetness and snow are determined by climatic conditions, so that a complete cycle of feedbacks is in operation (Figure 12.9).

The majority of modelling experiments so far have focused on the effect of land surface properties on climate predictability, beginning with the early atmospheric GCM study of Shukla and Mintz (1982) in which simulations were made with the model's land surface constrained to produce no evapotranspiration (desiccated case) or for the evapotranspiration to take place at the potential rate (saturated case), over the whole globe. They found that, in the desiccated case, there is almost no rainfall

over the extratropical continents in boreal summer, and an increase in the rainfall over South-east Asia and India due to the large moisture flux convergence from the oceans. They interpreted their results to indicate that dry soil at the beginning of the summer would lead to anomalously low rainfall in the extratropical summer season.

The 'memory' effect of soil wetness is frequently invoked as the underlying mechanism for its role in predictability. Delworth and Manabe (1988, 1989), using an atmospheric GCM with a simple 'bucket' model of soil moisture, showed that soil wetness 'reddens' the spectrum of climate variability. More sophisticated models incorporating a model of the biosphere (Sellers *et al.*, 1986; Sato *et al.*, 1989) were used to show that soil wetness anomalies can persist much longer than previously thought, and that the climate is quite sensitive to variations in soil wetness.

Atlas *et al.* (1993) and Fennessy and Shukla (1999) showed that the initial soil wetness anomalies present in extreme drought (e.g. 1988) or flood (e.g. 1993) summers in North America contribute to the subsequent summer rainfall with persistent soil wetness anomalies, dry (wet) rainfall anomalies and warm (cold) surface temperature occurring with dry (wet) soil wetness anomalies. For example, Figures 12.10 and 12.11 (taken from Fennessy and Shukla, 1999) show that an initial soil wetness anomaly on 1 June (Figure 12.10) can persist for up to a season, in some regions, and have a significant impact on the evaporation (Figure 12.11) and surface air temperature (not shown). They also found that the strength and nature of the impact of initial soil wetness anomalies on precipitation and surface temperature depend on several factors, including the extent and magnitude of the initial soil wetness anomaly, the strength of the solar forcing, the proximity to moisture sources, and the strength of the regional atmospheric circulation. They interpreted their results to suggest that seasonal atmospheric predictability could be increased by realistic initial soil wetness.

It has recently been shown that the sensitivity of precipitation to soil wetness is regionally localised. Koster *et al.* (2004) used 10 different land surface models in the Global Land–Atmosphere Coupling Experiment (GLACE) to show that the coupling strength between the atmosphere and the land surface is a strong function of location. Koster *et al.* (2004) identified the areas where this coupling is strong, and therefore has a strong bearing on the variability of precipitation, during boreal summer. The places where the coupling is strong, referred to as 'hot spots', are primarily transition zones between dry and wet climatic zones where the evaporation is large and sensitive to soil moisture and where the boundary layer moisture can trigger convection in the atmosphere.

12.3.3 Ocean–atmosphere–land influences (monsoon predictability)

The monsoon circulation is a dramatic example of the combined ocean, land and atmospheric effects; therefore, an estimate of the limit of monsoon predictability

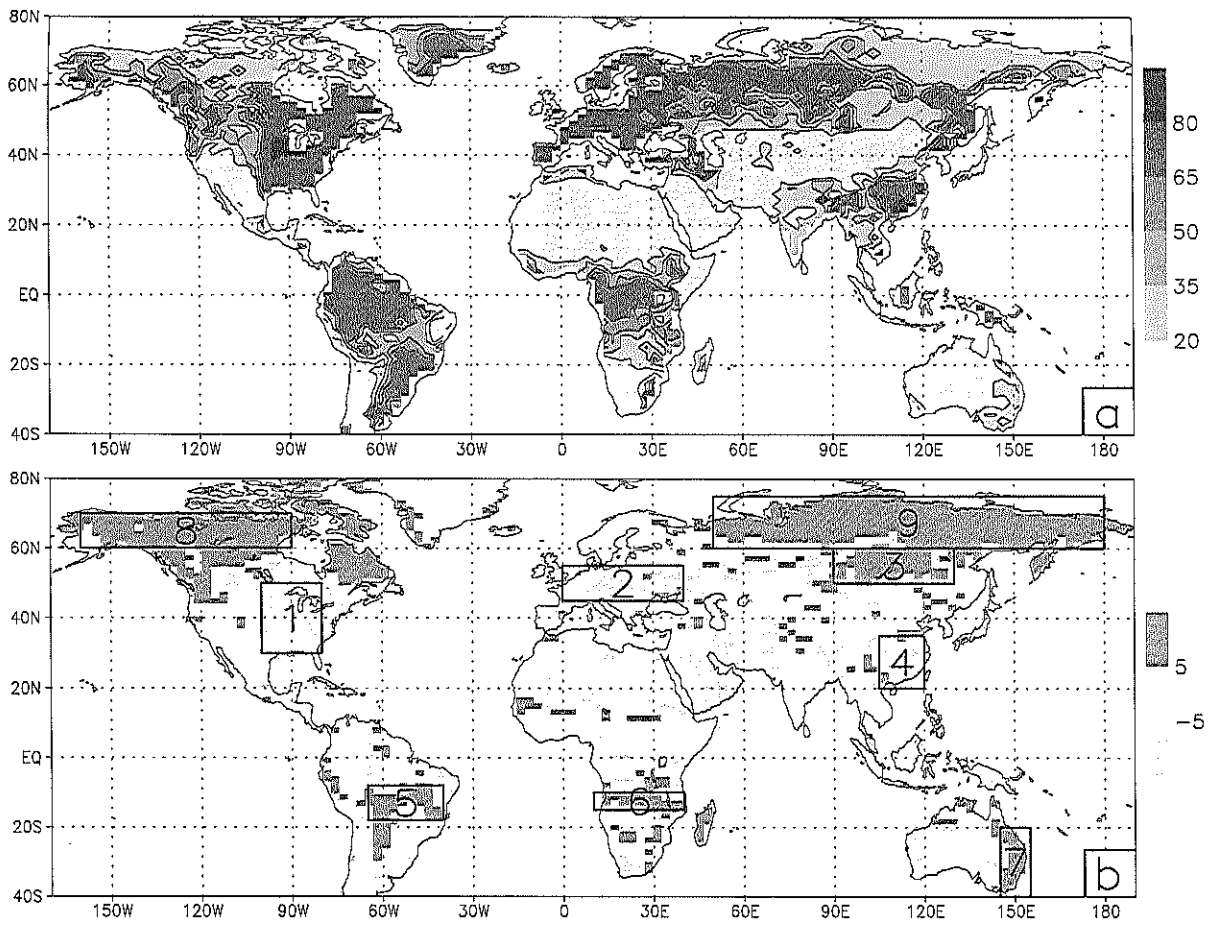

Figure 12.10 (a) Soil wetness climatology (% of saturation) for 1 June used to initialise atmospheric GCM ensembles and (b) initial soil wetness difference between ensembles initialised with observed soil wetness and those initialised with climatological soil wetness. Regions with differences greater/less than 10% of saturation are shaded dark/light. Numbered regions were used in a separate analysis (Fennessy and Shukla, 1999).

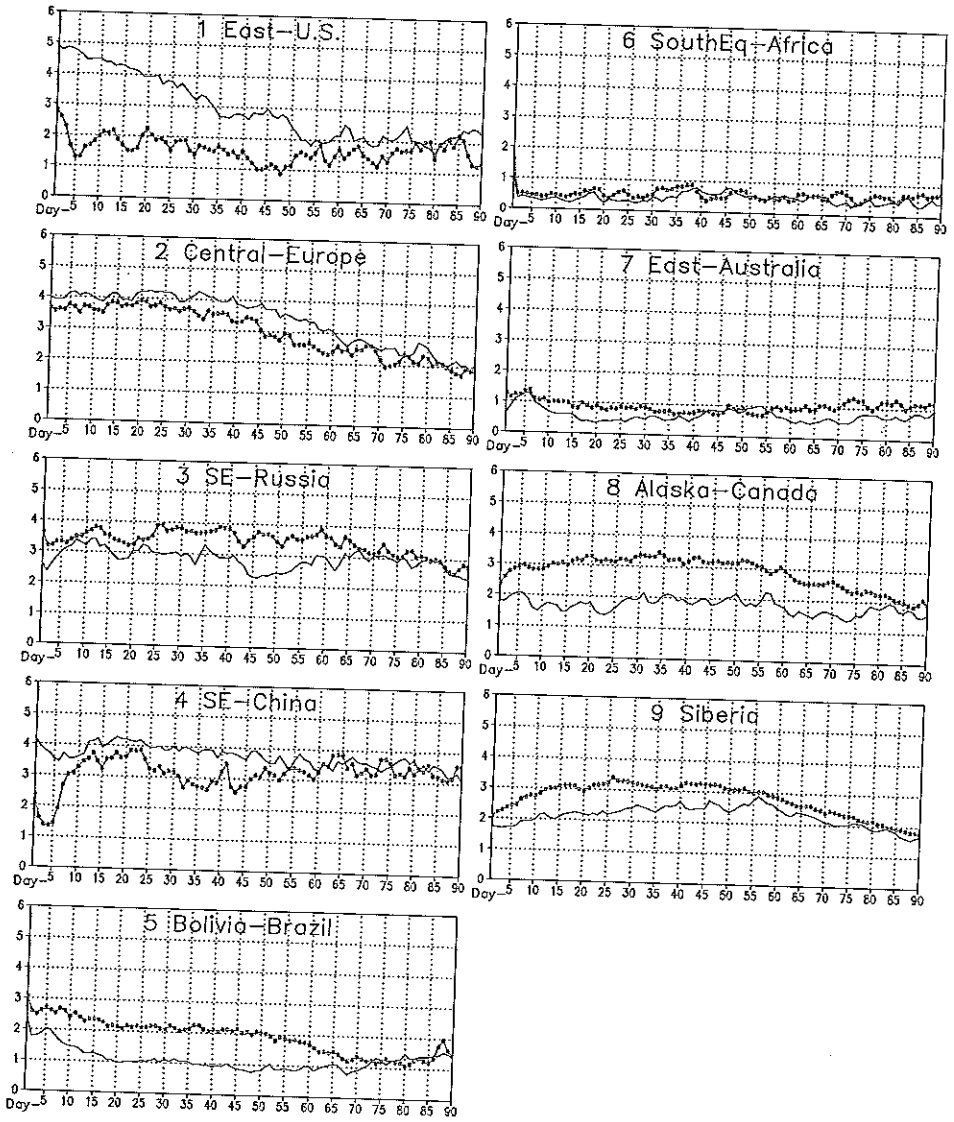

Figure 12.11 Area-averaged daily time series of evaporation for nine study regions shown in Figure 12.10(b) for control ensemble (solid) and observed initial soil wetness ensemble (dotted). Units are mm per day.

requires a clear understanding of the atmosphere–land interaction, atmosphere–ocean interaction, and the internal dynamics of the atmosphere alone. It was suggested by Charney and Shukla (1977) and later shown by Charney and Shukla (1981) that the large-scale, seasonal mean monsoon rainfall over India is largely determined by the boundary conditions over land and ocean. This was based on the observed relationship between Eurasian snow cover and monsoon rainfall (Blanford, 1884) and tropical

ocean temperature and Indian monsoon rainfall (Sikka, 1980; Rasmusson and Carpenter, 1983). However, it is well known that there is a large intraseasonal variability of the regional rainfall in the monsoon region during the monsoon season. Therefore, in a simple conceptual model, the seasonal mean monsoon rainfall over any small region can be considered to consist of two components: one large-scale seasonally persistent component and one relatively small-scale intraseasonal component (Krishnamurthy and Shukla, 2001). The large-scale seasonally persistent component can be attributed to ocean and/or land surface effects and the intraseasonal component to the internal dynamics of the atmosphere. The predictability of the seasonal mean for any given season depends on the relative magnitude of the two components. Even in the presence of large boundary forcing (namely SST anomalies in 1997), if the large-scale effect is small and the intraseasonal variations are large, the seasonal mean will not be predictable. To the extent that the seasonal mean anomalies are determined by the sampling of intraseasonal variations of rainfall, and if the intraseasonal variations were independent of the boundary forcing, the seasonal mean anomalies would not be predictable. It has also not been possible either to make dynamical predictions of seasonal mean rainfall or even to make reliable estimates of the monsoon rainfall, because of various limitations in models and modelling strategies. For example, models of the monsoon circulation and rainfall have large systematic errors in the mean and variance. The current atmospheric GCM experiments in which models are forced by prescribed SST are inadequate to capture the coupled ocean–atmosphere variability, and the current models do not have adequate treatment of land surface processes. The models are also not able to simulate the intraseasonal variability over the monsoon region.

An estimate of monsoon predictability using coupled ocean–atmosphere models is even more problematic, because the coupled models have even larger systematic errors in simulating the mean climate and its variability. If the coupled model cannot capture the march of the annual cycle in SST in the Indian Ocean and the surrounding areas, it is nearly impossible to get a reasonable simulation of monsoon circulation.

12.4 Predictability of coupled system

In the previous section, we described the predictability of the tropical atmosphere with prescribed SST. In similar experiments with an ocean model (B. Huang, personal communication), it was shown that the tropical upper ocean circulation and temperature are largely determined by the overlying atmospheric forcing. When an ocean model with completely different initial conditions (for 1982 and 1988) was forced by the atmospheric fluxes of 1982–3, the resulting tropical SST anomalies were indistinguishable from each other after 3–4 months. These experiments suggest that the tropical atmosphere is highly predictable for prescribed SST and the tropical ocean is highly predictable for prescribed atmospheric fluxes. However, these results

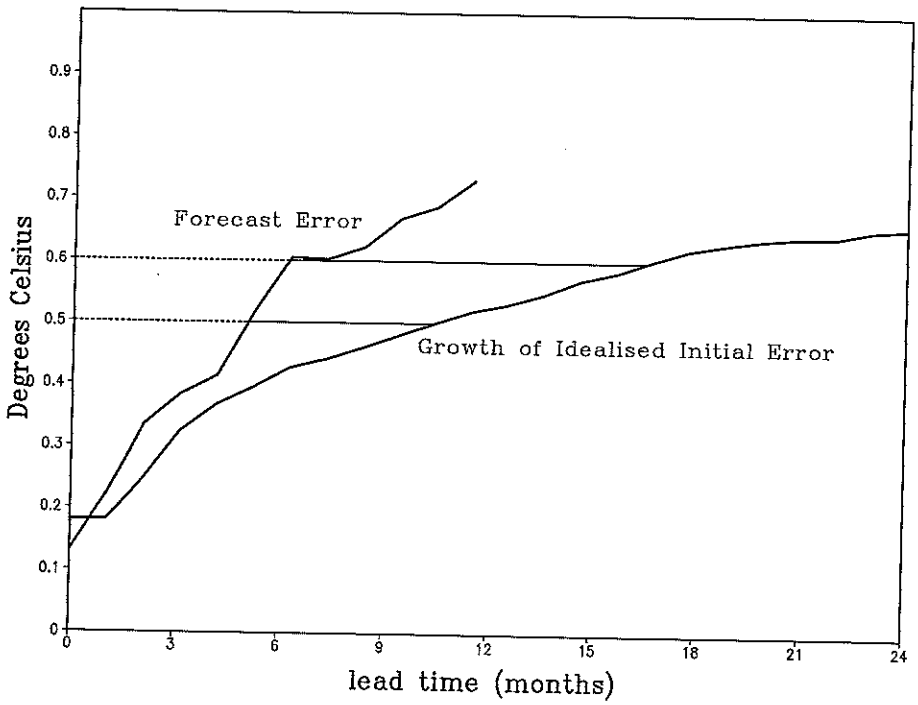

Figure 12.12 COLA anomaly coupled GCM NINO-3.4 forecast root mean squared error as a function of lead time. The forecast error is calculated based on 480 six member ensemble hindcasts initialised each January, April, July and October from 1981 to 2000 (see Kirtman, 2003, for details). The idealised NINO-3.4 root-mean-squared error growth is based on a multi-century simulation of the COLA anomaly coupled GCM (see Kirtman *et al.*, 2002) using an analogue approach to estimate the growth of initial errors.

do not necessarily imply that the coupled system is also as highly predictable as the individual components of the atmosphere and ocean. To estimate the predictability of the coupled ocean–atmosphere system is one of the major current challenges of climate research.

An estimate of the growth of initial error in the Zebiak–Cane coupled ocean–atmosphere model (Zebiak and Cane, 1987) was made by Goswami and Shukla (1991), and it was found that the coupled system is characterised by two timescales. One had an initial error doubling time of four months and the other had a doubling time of 15 months. In a more recent calculation, B. P. Kirtman (personal communication; Figure 12.12), using a global anomaly coupled ocean–atmosphere model, found that an initial error of about 0.2 K in the NINO-3.4 index of tropical Pacific SST takes about five months to double. Comparing the evolution of the forecast model's error with the growth of idealised initial errors in an 'identical twin' experiment, it was found that the forecast model reaches the same level of error in five months that is only reached after 10 months of idealised error growth. This suggests that there is substantial room for improving the prediction of tropical SST in a coupled model.

We do not yet have a clear understanding of mechanisms that determine the amplitude and the life cycle of ENSO. For example, we do not know whether ENSO should be considered to be a manifestation of an unstable oscillator, or whether it should be considered a stochastically forced damped linear system. The observations for the past 50 years can support both theories. We also do not understand the role of weather noise in the initiation and growth of ENSO events. A better understanding of ENSO dynamics, and improved methods of initialising models of the coupled ocean–atmosphere system for ENSO prediction are required before we can make reliable estimates of the predictability of ENSO.

12.4.1 Case study

A low-resolution coupled ocean–atmosphere model, a moderate-resolution atmospheric GCM and a high-resolution nested regional climate model were used to produce six-month lead forecasts for the boreal winter of 1997–8. The procedure for producing forecasts of the tropical SST anomaly, the global atmospheric circulation and precipitation and the regional climate anomalies over North America is shown schematically in Figure 12.13. It should be noted that this experimental strategy was devised only to overcome the problem of insufficient computer time to integrate high-resolution global coupled models. Briefly, the tropical Pacific SST pattern was predicted for up to 18 months in advance using the coupled ocean–atmosphere model with available input data at the time of the forecast (Kirtman *et al.*, 1997). Multiple realisations of the coupled model forecast were averaged to produce an ensemble-mean SST forecast that was then statistically extended to predict the global SST anomaly. The latter was added to an observed climatology for global SST and used as a lower boundary condition for an ensemble of integrations of the global atmospheric GCM. Each of the global model integrations was used to provide the lateral boundary conditions for a companion integration of a regional climate model. The ensembles of global and regional model predictions were made at least six months prior to the verification time of the forecasts.

12.4.2 The tropical Pacific SST forecast

The SST forecast produced by the anomaly coupled model and subsequent statistical projections called for a continuation of the unprecedented, anomalously warm surface temperature in the tropical eastern and central Pacific through boreal summer of 1998 with a peak amplitude in about December 1997 and January 1998, and diminishing thereafter. The predicted warmer than normal water in the Pacific was located east of the dateline along the equator and extended about 5–10° north and south of the equator. The peak SST value forecast by this model was about 3 °C above normal.

Up to the time that the forecast was made, during the ENSO warm event (through September 1997), the model had been quite accurate in predicting the onset and

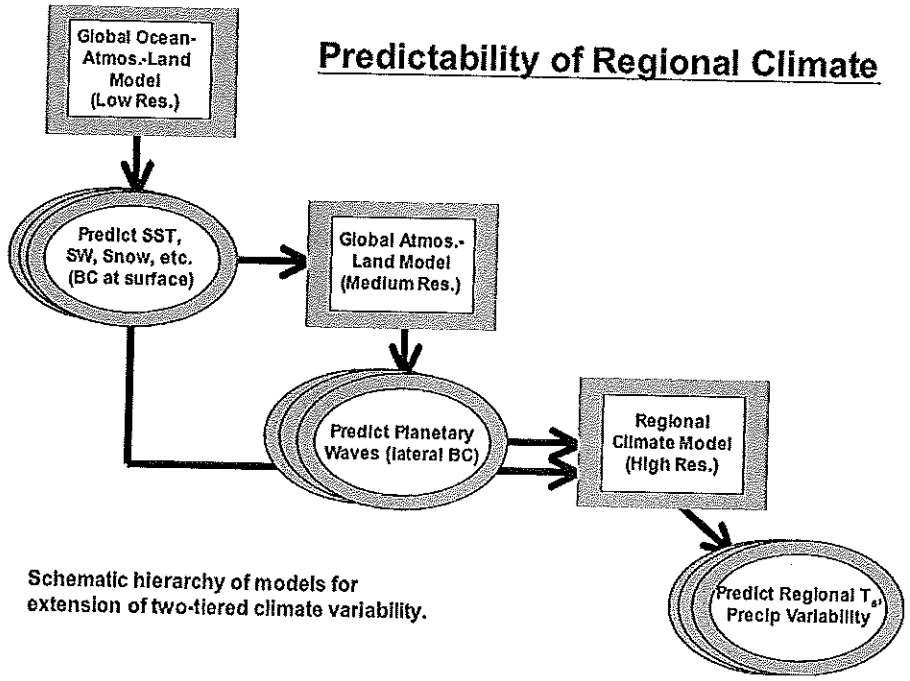

Figure 12.13 Schematic diagram showing the multitiered prediction system. At upper left is the global coupled ocean–atmosphere–land model run at low resolution to generate an ensemble of predicted SST, snow and other boundary conditions (BC) at the surface. These are then used as boundary conditions for both a global atmospheric model run at medium resolution, used to generate an ensemble of predictions of the large-scale circulation in the atmosphere, and a regional climate model run at high resolution to generate an ensemble of predictions of regional variations in surface temperature and precipitation. The large-scale circulation predicted by the medium resolution global atmospheric model is also used as a lateral boundary condition in the regional climate model.

rapid increase of the SST anomaly, although its prediction of the magnitude of the maximum anomaly was substantially smaller than observed. The JFM98 forecast made six months in advance was quite accurate in terms of amplitude, phase relative to the annual cycle and spatial pattern. The predicted maximum anomaly was west of the observed maximum and fell short of the observed amplitude by about 1 °C. Compared with similar predictions and simulations made prior to this one, the forecast was considered to be quite accurate and generally deemed successful.

12.4.3 The atmospheric circulation in the winter hemisphere

The model-based SST forecast was applied as a lower boundary condition to the COLA atmospheric GCM to produce an ensemble of nine forecasts. The ensemble

members were generated by initialising the model with slightly different initial conditions to provide some measure of the uncertainty of the forecast. The COLA model ensemble mean forecast was quite skilful, comparable to the result shown in Figure 12.5.

12.4.4 Precipitation over North America

Typically, predictions of precipitation are less reliable than temperature forecasts due to the fact that precipitation is more variable, has a smaller spatial correlation scale and is non-normally distributed. Nevertheless, the large-scale characteristics of precipitation anomalies are known to be correlated with those of other fields and some information may be obtained from predictions of seasonal mean precipitation. The seasonal mean precipitation anomaly for January through March 1998 is shown in Figure 12.14: the prediction made by the global model is in the top panel, the observations (Xie and Arkin, 1996) are in the middle panel, and the prediction made using the nested Eta80 model is in the bottom panel. The main features of the predicted anomaly pattern are a swath of positive anomalies to the south and a band of negative anomalies to the north. The positive anomalies (more than 0.5 mm per day or 50 mm for the entire season above normal) extend from the Pacific north-west states of the USA, through California and the south-west USA into Mexico, and along the Gulf of Mexico into the south-east USA. The band of negative departures from normal extends from the Pacific coast of Canada through the northern plains and Great Lakes states of the USA into the maritime provinces of Canada.

This relatively limited case study shows that by employing an ensemble of models it is possible to make useful predictions of the evolution of the large SST anomalies that can have a large effect on the tropical and extratropical climate up to seasons in advance. Furthermore, these SST predictions can be used in a tier-2 system (e.g. Mason *et al.*, 1999; Goddard *et al.*, 2003) to force a reasonably good atmospheric GCM to produce predictions of the large-scale atmospheric circulation. A nested regional climate model can then be used to resolve important details of the topography and the solution itself to further constrain the forecast precipitation field and make useful six-month lead predictions of regional seasonal mean precipitation anomalies.

12.5 Predictability of seasonal variations in a changing climate

The observed current climate changes are a combination of anthropogenic influences and the natural variability. In addition to possible anthropogenic influence on climate due to changing the atmospheric composition, it is quite likely that land use in the tropics will undergo extensive changes, which will lead to significant changes in the

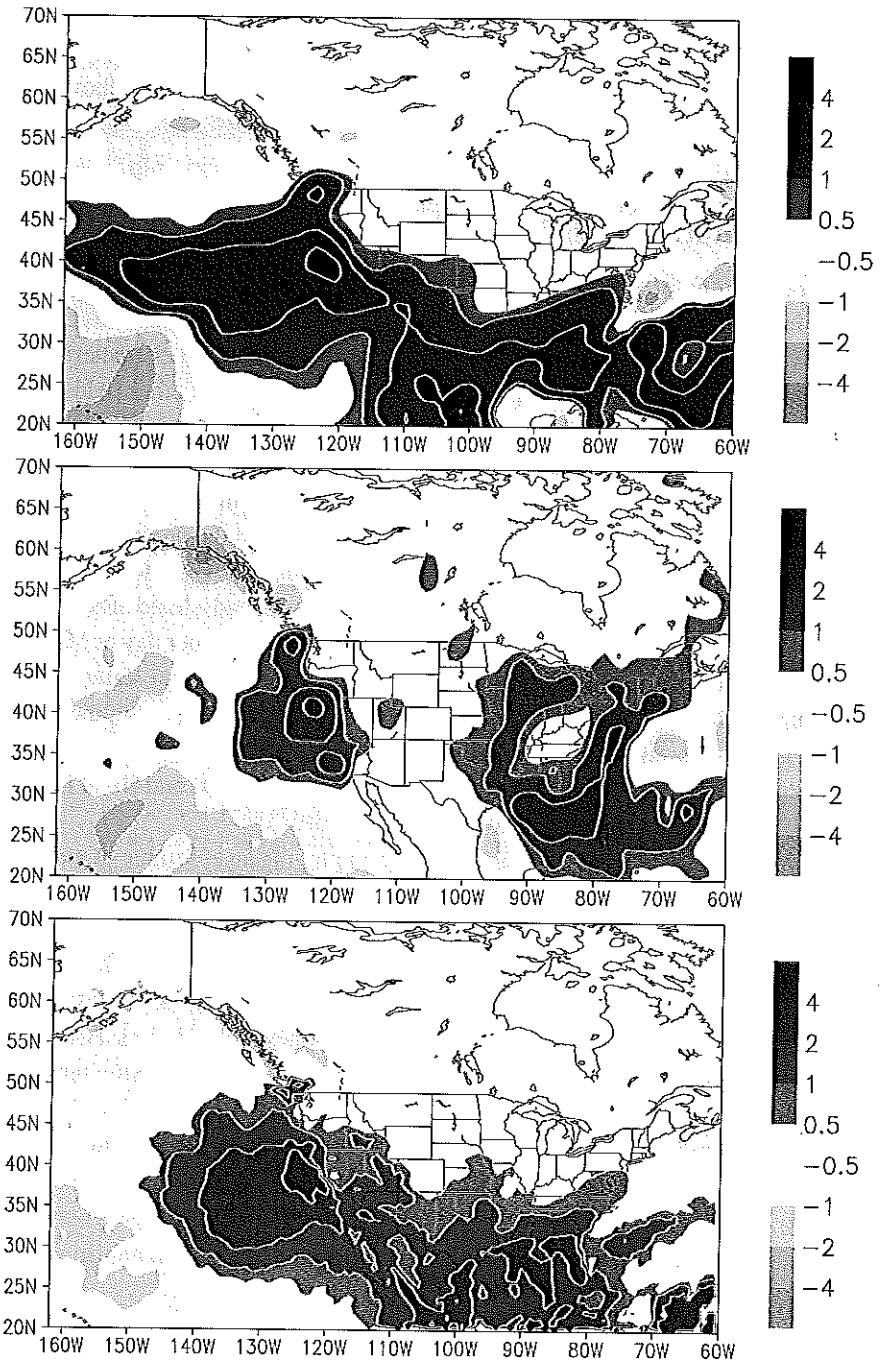

Figure 12.14 Seasonal mean precipitation anomaly over North America for January–March 1998 case. (Top) COLA atmospheric GCM ensemble mean. (Middle) Observed. (Bottom) Eta80 nested in COLA atmospheric GCM.

biophysical properties of the land surface. There is a scientific basis and a plausible mechanism for the contention that these land use changes could have significant remote influences on the climate system, and in the case of Amazon land use change, on ENSO variability in particular (Hu *et al.*, 2004). The dominant effects of changes in the land surface appear to be due to changes in the albedo and soil wetness.

The role of SST variability on the atmosphere and land in the last century, including problems such as the variability and predictability of ENSO and the ENSO/monsoon relationship have been investigated in the Climate of the 20th Century (C20C; Folland *et al.*, 2002) project using SST specified from analysis of existing data. It has been shown, for example, that the general increase in SST in the eastern tropical Indian and Pacific Oceans has led to an increase in the predictability of seasonal variations (I.-S. Kang, personal communication). This can be projected in future climate scenarios using variants of the C20C approach, in which the SST is specified from coupled GCM climate change projections. This 'two-tier' approach can illuminate the atmospheric and land surface response to the SST variability. However, it is of limited value in helping to understand the changes in the SST variability itself. A coupled approach is needed for this part of the problem.

12.6 Factors limiting seasonal predictability

Estimates of seasonal predictability are model dependent. For example, the estimates of seasonal predictability have changed considerably as the models have evolved. In Figure 12.15, the response to ENSO forcing simulated by various versions of an atmospheric GCM, as it evolved over a 20-year period, is shown. It is clear that the fidelity of the simulation, and consequently the estimate of predictability, has changed markedly over the two decades of model development. Even at this late stage of model development, model differences give rise to very large differences in estimates of predictability. Figure 12.16 shows the probability distributions of geopotential height variance explained by tropical Pacific SST in the Pacific–North America region produced by six different atmospheric GCMs, based on ensembles of simulations. Current state-of-the-art models may underestimate or overestimate the variance explained by as much as a factor of two, and there is even some variation in the spread of the models' distributions of this quantity. This is a direct consequence of the uncertainty in the models' parametrisations of subgrid-scale processes, especially convection. As shown in Figure 12.17, the six models used to produce Figure 12.16 have significantly different rainfall variance in the tropical Pacific, where the atmospheric response to SST anomalies is most sensitive. The range of rainfall variance among the models is up to a factor of 8.

Another major factor limiting progress in understanding seasonal predictability is the limited size of ensembles employed. The problem of seasonal prediction is a probabilistic one, and the simple way in which this is addressed in current prediction

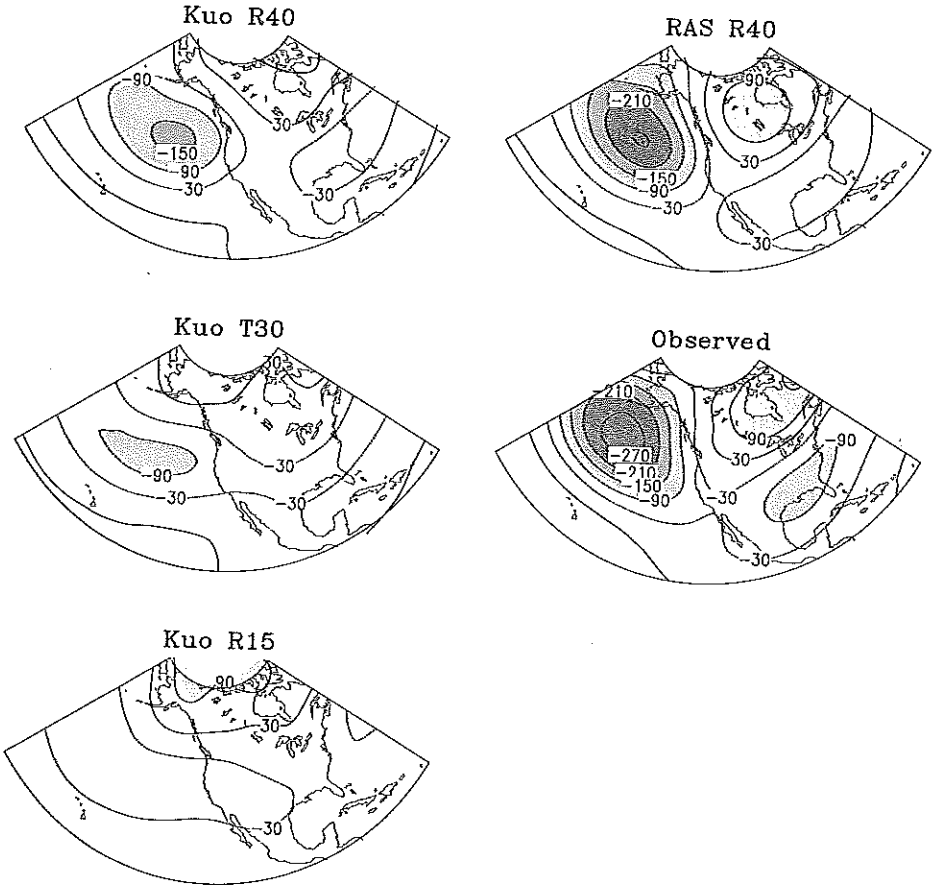

Figure 12.15 Some simulations of the difference in Jan–Feb–March mean 500 hPa geopotential height for 1983 (a year with warm SST anomalies in the eastern tropical Pacific) minus 1989 (a year with cold SST anomalies in the eastern tropical Pacific). The simulations are done with various versions of the same atmospheric GCM. (Left) Atmospheric GCM simulations with the Kuo parametrisation of cumulus convection: top, R40 horizontal resolution; middle, T30 horizontal resolution; bottom, R15 horizontal resolution. (Upper right) Atmospheric GCM simulation with RAS parametrisation of cumulus convection and R40 horizontal resolution. (Lower right) Observed difference computed using NCEP/NCAR reanalysis fields.

systems is to build ensembles of model integrations that are intended to sample the uncertainty in the initial conditions. It has been shown that fairly large ensembles are needed for cases with weak or moderate tropical forcing (Straus and Molteni, 2004). It has also been shown that the use of multiple models in an ensemble is more effective than using multiple realisations with a single model (Palmer *et al.*, 2004; T. Palmer, personal communication). The latter finding is probably because multiple

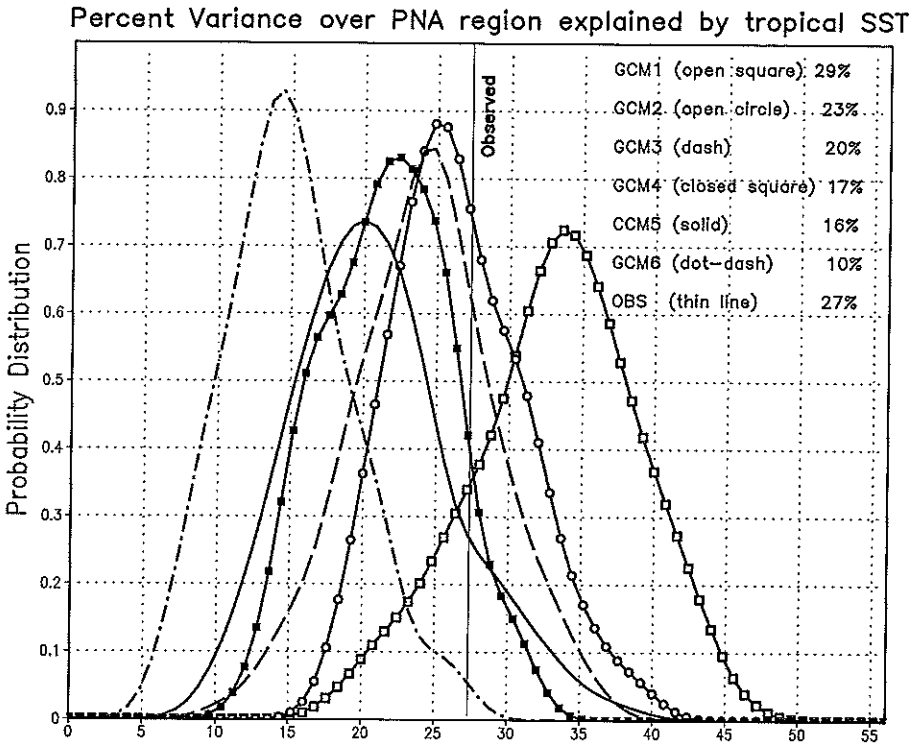

Figure 12.16 Probability distributions of (area-averaged) temporal variance of winter mean 500 hPa height explained by an observed tropical Pacific SST time series from 100 'samples' of seasonal simulations with various atmospheric GCMs. The SST time series is obtained from the leading mode of a singular value decomposition of observed tropical Pacific SST with 500 hPa height over the Pacific–North America region obtained from the NCEP reanalysis for the winters January–March 1968–97. Each GCM sample was formed from an ensemble of winter simulations for the winters of 1983–93 by picking one member of the ensemble at random for each year. The temporal variance explained by the SST time series was averaged over the Pacific–North America region (180°–60° W).

models sample the uncertainty in the physical parametrisations, and due to a non-linear interaction between the individual models' systematic error and the predictable signal. The requirement for large ensembles with multiple climate models has only been lightly explored, primarily due to limited computational resources.

A third barrier to progress is the difficulty with initialising coupled ocean–atmosphere–land models. Atmospheric data assimilation has reached a mature stage that is demonstrably extracting a large fraction of the usable information from the available observations (Simmons and Hollingsworth, 2002). Similarly, ocean data assimilation has made great strides in the recent decade, and new ocean observing systems hold the promise of providing a more complete representation of the ocean state, at least for the upper 500 m (Derber and Rosati, 1989; Ji *et al.*, 1995). The assimilation of land surface observations has only recently been attempted globally

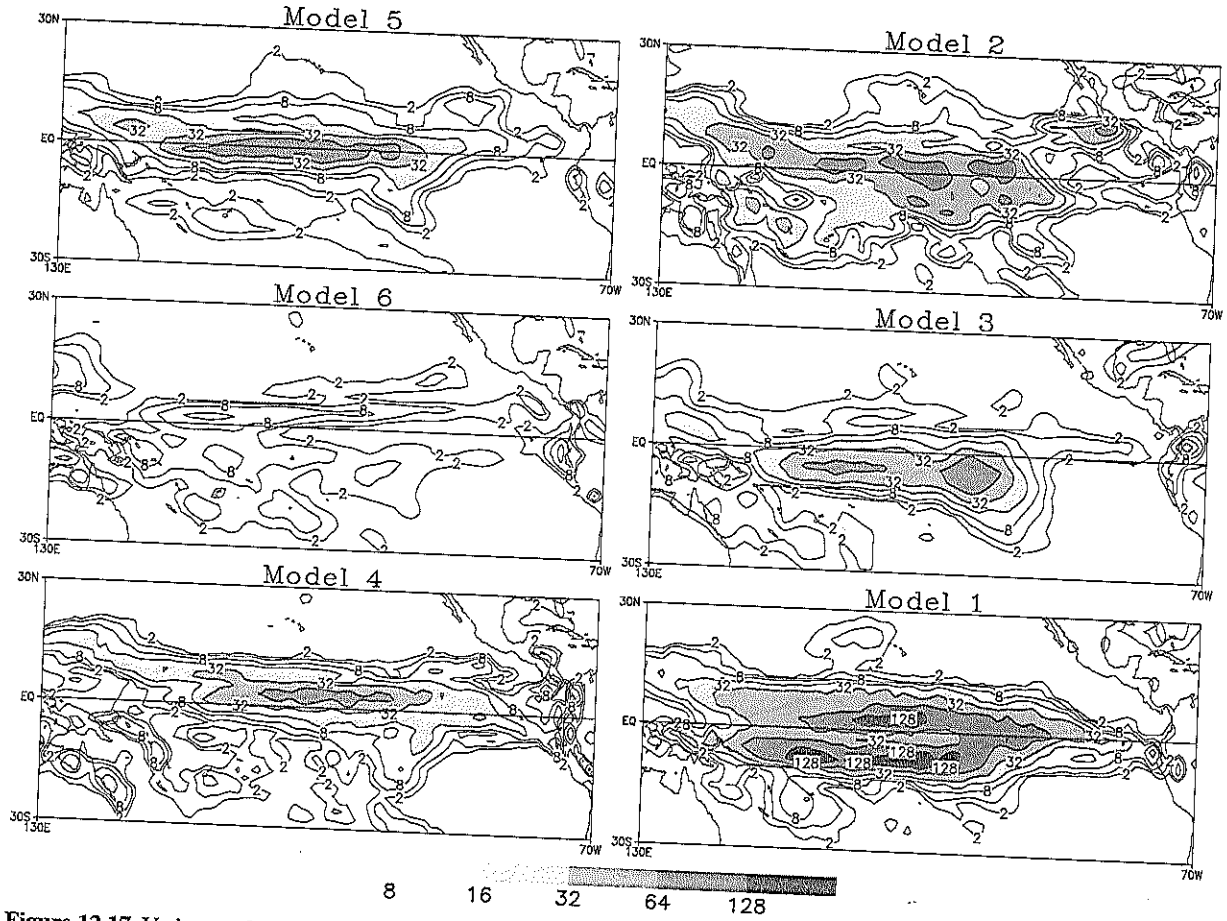

Figure 12.17 Variance of precipitation for the same six models used for Figure 12.16.

(Dirmeyer, 2000), so we have only a limited understanding of how well we are initialising land surface conditions. Furthermore, the systematic errors in the seasonal prediction models make the evolution of soil moisture from its initial state problematic. Most importantly, the climate system is known to have modes of variability that depend on the couplings between ocean and atmosphere and land and atmosphere, but these modes are not necessarily being initialised in the process of initialising the components of the coupled model.

12.7 Summary and prospects for the future

Improvements in dynamical weather prediction over the past 30 years did not occur because of any major scientific breakthroughs in our understanding of the physics or dynamics of the atmosphere. Dynamical weather prediction is challenging: progress takes place slowly and through a great deal of hard work that is not necessarily scientifically stimulating, performed in an environment that is characterised by frequent setbacks and constant criticism by a wide range of consumers and clients. Nevertheless, scientists worldwide have made tremendous progress in improving the skill of weather forecasts by advances in data assimilation, improved parametrisations, improvements in numerical techniques and increases in model resolution and computing power.

The growth rate of initial errors in NWP models is well known, and the current limits of predictability of weather are well documented. The most promising way to improve forecasts for days 2–15 is to improve the forecast at day 1. During the past 25 years, the weather forecast error at day 1 has been reduced by more than 50%. At present, forecasts for day 4 are, in general, as good as forecasts for day 2 made 25 years ago. With improved observations, better models and faster computers, it is reasonable to expect that the forecast error at day 1 will be further reduced.

There is a scientific basis for extending the successes of NWP to climate prediction. A model's ability to reliably predict the sequential evolution of the climate system depends on the model's ability to simulate the statistical properties of the observed climate system. There is sufficient evidence to indicate that, as models improve in their representation of all the statistical properties of the observed climate, they also improve in their prediction skill of the evolution of climate anomalies.

Until 25 years ago, a dynamical seasonal climate prediction was not conceivable. Over the past 25 years, steadily progressing dynamical seasonal climate prediction has achieved a level of skill that is considered useful for some societal applications. However, such successes are limited to periods of large, persistent anomalies at the Earth's surface. There is significant unrealised seasonal predictability. Progress in dynamical seasonal prediction in the future depends critically on improving coupled ocean–atmosphere–land models, improving observations, and increasing the ability to assimilate those observations. The current generation of ENSO prediction models

is able to predict the average SST over the equatorial Pacific, but not the evolution and amplitude of an individual ENSO event.

Currently, about 10 centres worldwide are making dynamical weather forecasts every day with a lead time of 5–15 days with about 5–50 ensemble members, so that there are about 500 000 daily weather maps that can be verified each year. It is this process of routine verification by a large number of scientists worldwide, followed by attempts to improve the models and data assimilation systems, that has been the critical element in the improvement of dynamical weather forecasts. In contrast, if we assume that dynamical seasonal predictions, with a lead time of 1–3 seasons, could be made by 10 centres worldwide every month, each with 10–20 ensemble members, there would be fewer than 5000 seasonal mean predictions worldwide that could be verified each year. This is a factor of 100 fewer cases than are available for advancing NWP, so improvement in dynamical seasonal prediction might proceed at a pace that is much slower than that for NWP if we don't do something radically different.

It is suggested that, for accelerating progress in dynamical seasonal prediction, we reanalyse and reforecast the seasonal variations for the past 50 years, every year. This will entail annually reanalysing the observations of the atmosphere and ocean available since 1950, and making an ensemble of six-month lead forecasts, starting from initial conditions in each month of the ~50-year period. By doing so, we will exercise state-of-the-art coupled ocean–atmosphere–land models and data assimilation systems for a large number of seasonal prediction cases and verify them against observations. We should also conduct model development experiments (sensitivity to parametrisations, resolution, coupling strategy, etc.) with the specific goal of reducing seasonal prediction errors.

Acknowledgements

We would like to thank several people at the Center for Ocean–Land–Atmosphere Studies who made contributions to this paper, either through the preparation of figures or discussions. B. Kirtman and M. Fennessy provided Figures 12.12 and 12.13, respectively, and Tim DelSole, Paul Dirmeyer, Larry Marx, Dan Paolino, and David Straus helped with both the figures and the text.

References

Alexander, M. A. and C. Deser (1995). A mechanism for the recurrence of wintertime midlatitude SST anomalies. *J. Phys. Oceanogr.*, **25**, 122–37.

Atlas, R., N. Wolfson and J. Terry (1993). The effect of SST and soil moisture anomalies on GLA model simulations of the 1988 U.S. summer drought. *J. Climate*, **6**, 2034–48.

Bamzai, A. and L. Marx (2000). COLA AGCM simulation of the effect of anomalous spring snow over Eurasia on the Indian summer monsoon. *Quart. J. Roy. Meteor. Soc.*, **126**, 2575–84.

Barnett, T. P., L. Dumenil, U. Schlese and E. Roeckner (1988). The effect of Eurasian snow cover on global climate. *Science*, **239**, 504–7.

Barnston, A. G. and R. E. Livezey (1987). Classification, seasonality and persistence of low-frequency atmospheric circulation patterns. *Mon. Wea. Rev.*, **115**, 1083–126.

Bhatt, U. S., M. A. Alexander, D. S. Battisti, D. D. Houghton and L. M. Keller (1998). Atmosphere–ocean interaction in the North Atlantic: near-surface climate variability. *J. Climate*, **11**, 1615–32.

Blanford, H. F. (1884). On the connexion of the Himalayan snowfall with dry winds and seasons of droughts in India. *Proc. Roy. Soc. Lond.*, **37**, 3–22.

Charney, J. (1966). Some remaining problems in numerical weather prediction. In *Advances in Numerical Weather Prediction*, pp. 61–70. Hartford, CT: Travelers Research Center.

(1975). Dynamics of deserts and droughts in the Sahel. *Quart. J. Roy. Meteor. Soc.*, **101**, 193–202.

Charney, J. G. and J. Shukla (1977). Predictability of monsoons. *Joint IUTAM/IUGG Symposium on Monsoon Dynamics* (5–9 December, 1977), New Delhi, India.

(1981). Predictability of monsoons. In *Monsoon Dynamics*, ed. J. Lighthill and R. P. Pearce, pp. 99–109. Cambridge University Press.

Charney, J., R. G. Fleagle, H. Riehl, V. E. Lally and D. Q. Wark (1966). The feasibility of a global observation and analysis experiment. *Bull. Amer. Meteor. Soc.*, **47**, 200–20.

Cohen, J. and D. Rind (1991). The effect of snow cover on climate. *J. Climate*, **4**, 689–706.

Delworth, T. L. and S. Manabe (1988). The influence of potential evaporation on the variabilities of simulated soil wetness and climate. *J. Climate*, **1**, 523–47.

(1989). The influence of soil wetness on near-surface atmospheric variability. *J. Climate*, **2**, 1447–62.

Derber, J. and A. Rosati (1989). A global oceanic data assimilation system. *J. Phys. Oceanogr.*, **19**, 1333–47.

Dickinson, R. E. (1984). Modelling evapotranspiration for three-dimensional global climate models. In *Climate Processes and Climate Sensitivity*, pp. 58–72. Geophysical Monograph **29**, Maurice Ewing Vol. 5. American Geophysical Union.

Dirmeyer, P. A. (2000). Using a global soil wetness data set to improve seasonal climate simulation. *J. Climate*, **13**, 2900–22.

Dirmeyer, P. A. and J. Shukla (1993). Observational and modeling studies of the influence of soil moisture anomalies on atmospheric circulation (review). In *Prediction of Interannual Climate Variations*, ed. J. Shukla, pp. 1–24. NATO ASI Series I: Global Environmental Change, Vol. 6.

(1996). The effect on regional and global climate of expansion of the world's deserts. *Quart. J. Roy. Meteor. Soc.*, **122**(530), 451–82.

Fennessy, M. J. and J. Shukla (1999). Impact of initial soil wetness on seasonal atmospheric prediction. *J. Climate*, **12**, 3167–80.

Fennessy, M. J., L. Marx and J. Shukla (1985). General circulation model sensitivity to 1982–83 equatorial Pacific sea surface temperature anomalies. *Mon. Weather Rev.*, **115**, 858–64.

Folland, C. K., J. Shukla, J. L. Kinter III and M. J. Rodwell (2002). C20C: the Climate of the Twentieth Century project. *CLIVAR Exchanges*, **7**, 37–9. (Available from International CLIVAR Project Office, Southampton Oceanography Centre, Empress Dock, Southampton, SO14 3ZH, UK; (www.clivar.org/publications/exchanges/ex24/ex24.pdf)

Goddard, L., A. G. Barnston and S. J. Mason (2003). Evaluation of the IRI's "Net Assessment" seasonal climate forecasts: 1997–2001. *Bull. Am. Meteorol. Soc.*, **84**, 1761–81.

Goswami, B. N. and J. Shukla (1991). Predictability of a coupled ocean-atmosphere model. *J. Climate*, **3**, 2–22.

Gutzler, D. S. and J. Shukla (1984). Analogs in the wintertime 500 mb height field. *J. Atmos. Sci.*, **41**, 177–89.

Hahn, D. G. and S. Manabe (1975). The role of mountains in the south Asian monsoon circulation. *J. Atmos. Sci.*, **32**, 1515–41.

Hahn, D. and J. Shukla (1976). An apparent relationship between Eurasia snow cover and Indian monsoon rainfall. *J. Atmos. Sci.*, **33**, 2461–3.

Hess, P. and H. Brezowsky (1969). Katalog der Grosswetterlagen Europas. *Ber. Dt. Wetterd.*, **15**.

Hu, Z.-Z., E. K. Schneider, U. Bhatt and B. P. Kirtman (2004). Potential for influence of land surface processes on ENSO. *J. Geophys. Res.*, **109**.

Ji, M., A. Leetmaa and J. Derber (1995). An ocean analysis system for seasonal to interannual climate studies. *Mon. Weather Rev.*, **123**, 460–81.

Kinter III, J. L., J. Shukla, L. Marx and E. Schneider (1988). A simulation of the winter and summer circulation with the NMC global spectral model. *J. Atmos. Sci.*, **45**, 2486–522.

Kirtman, B. P. (2003). The COLA anomaly coupled model: ensemble ENSO prediction. *Mon. Weather Rev.*, **131**, 2324–41.

Kirtman, B. P., Y. Fan and E. K. Schneider (2002). The COLA global coupled and anomaly coupled ocean-atmosphere GCM. *J. Climate*, **15**, 2301–20.

Kirtman, B. P., J. Shukla, B. Huang, Z. Zhu and E. K. Schneider (1997). Multiseasonal predictions with a coupled tropical ocean global atmosphere system. *Mon. Weather Rev.*, **125**, 789–808.

Koster, R. D., P. A. Dirmeyer, Z. Guo, *et al.* (2004). Regions of strong coupling between soil moisture and precipitation. *Science*, **305**, 1138–40.

Krishnamurthy, V. and J. Shukla (2001). Observed and model simulated interannual variability of the Indian monsoon. *Mausam*, **52**, 133–50.

Leith, C. E. (1971). Atmospheric predictability and two-dimensional turbulence. *J. Atmos. Sci.*, **28**, 148–61.

Leith, C. E. and R. H. Kraichnan (1972). Predictability of turbulent flows. *J. Atmos. Sci.*, **29**, 1041–58.

Lorenz, E. N. (1965). A study of the predictability of a 28-variable model. *Tellus*, **17**, 321–33.

(1969a). The predictability of a flow which possesses many scales of motion. *Tellus*, **21**, 289–307.

(1969b). Atmospheric predictability as revealed by naturally occurring analogues. *J. Atmos. Sci.*, **26**, 636–46.

(1979). Forced and free variations of weather and climate. *J. Atmos. Sci.*, **8**, 1367–76.

(1982). Atmospheric predictability experiments with a large numerical model. *Tellus*, **34**, 505–13.

Mason, S. J., L. Goddard, N. E. Graham, E. Yulaeva, L. Sun and P. A. Arkin (1999). The IRI seasonal climate prediction system and the 1997/98 El Niño event. *Bull. Am. Meteorol. Soc.*, **80**, 1853–73.

Miyakoda, K., C. T. Gordon, R. Caverly, W. F. Stern, J. J. Sirutis and W. Bourke (1983). Simulation of a blocking event in January 1977. *Mon. Weather Rev.*, **111**, 846–69.

Moura, D. A. and J. Shukla (1981). On the dynamics of droughts in northeast Brazil: observations, theory and numerical experiments with a general circulation model. *J. Atmos. Sci.*, **38**, 2653–75.

Namias, J. (1969). Seasonal interactions between the North Pacific Ocean and the atmosphere during the 1960's. *Mon. Weather Rev.*, **97**, 173–92.

(1986). Persistence of flow patterns over North America and adjacent ocean sectors. *Mon. Weather Rev.*, **114**, 1368–83.

Nobre, C. A., P. J. Sellers and J. Shukla (1991). Amazonian deforestation and regional climate change. *J. Climate*, **4**, 957–88.

Palmer, T. N., A. Alessandri, U. Andersen, *et al.* (2004). Development of a European multi-model ensemble system for seasonal to inter-annual prediction (DEMETER). *Bull. Am. Meteorol. Soc.*, **85**, 853–72.

Palmer, T. N. and J. Shukla (2000). Editorial to DSP/PROVOST special issue. *Quart. J. Roy. Meteor. Soc.*, **126**, 1989–90.

Palmer, T. N. and Z. Sun (1985). A modelling and observational study of the relationship between sea surface temperature in the northwest Atlantic and the atmospheric general circulation. *Quart. J. Roy. Meteor. Soc.*, **111**, 947–75.

Randall, D., J. Curry, D. Battisti, *et al.* (1998). Status of and outlook for large-scale modeling of atmosphere–ice–ocean interactions in the Arctic. *Bull. Am. Meteorol. Soc.*, **79**, 197–219.

Rasmusson, E. M. and T. H. Carpenter (1983). The relationship between eastern equatorial Pacific sea surface temperatures and rainfall over India and Sri Lanka. *Mon. Weather Rev.*, **111**, 517–28.

Sato, N., P. J. Sellers, D. A. Randall, *et al.* (1989). Effects of implementing the Simple Biosphere model (SiB) in a general circulation model. *J. Atmos. Sci.*, **46**, 2757–82.

Sellers, P. J., Y. Mintz, Y. C. Sud and A. Dalcher (1986). A Simple Biosphere Model (SIB) for use within general circulation models. *J. Atmos. Sci.*, **43**, 505–31.

Shukla, J. (1975). Effect of Arabian sea-surface temperature anomaly on Indian summer monsoon: a numerical experiment with GFDL model. *J. Atmos. Sci.*, **32**, 503–11.

(1981a). Dynamical predictability of monthly means. *J. Atmos. Sci.*, **38**, 2547–72.

(1981b). *Predictability of the Tropical Atmosphere*. NASA Technical Memorandum 83829. Goddard Space Flight Center, Greenbelt, MD: NASA.

(1985). Predictability. In *Issues in Atmospheric and Oceanic Modeling. II: Weather Dynamics* ed. S. Manabe pp. 87–122. Advances in Geophysics 28B. Academic Press.

(1998). Predictability in the midst of chaos: a scientific basis for climate forecasting. *Science*, **282**, 728–31.

Shukla, J. and M. Fennessy (1988). Prediction of time mean atmospheric circulation and rainfall: influence of Pacific SST anomaly. *J. Atmos. Sci.*, **45**, 9–28.

Shukla, J. and Y. Mintz (1982). The influence of land-surface evapotranspiration on the earth's climate. *Science*, **214**, 1498–501.

Shukla, J. and B. N. Misra (1977). Relationships between sea surface temperature and wind speed over the Central Arabia Sea, and monsoon rainfall over India. *Mon. Weather Rev.*, **105**, 998–1002.

Shukla, J. and J. M. Wallace (1983). Numerical simulation of the atmospheric response to equatorial Pacific sea surface temperature anomalies. *J. Atmos. Sci.*, **40**, 1613–30.

Shukla, J., J. Anderson, D. Baumhefner, *et al.* (2000a). Dynamical seasonal prediction. *Bull. Am. Meteorol. Soc.*, **81**, 1–14.

Shukla, J., D. A. Paolino, D. M. Straus, *et al.* (2000b). Dynamical seasonal predictions with the COLA atmospheric model. *Quart. J. Royal. Meteor. Soc.*, **126**, 2265–91.

Sikka, D. R. (1980). Some aspects of the large-scale fluctuations of summer monsoon rainfall over India in relation to fluctuations in the planetary and regional scale circulation parameters. *Proc. Indian Acad. Sci.*, **89**, 179–95.

Simmons, A. J. and A. Hollingsworth (2002). Some aspects of the improvement in skill of numerical weather prediction. *Quart. J. Roy. Meteor. Soc.*, **128**, 647–77.

Simmons, A. J., R. Mureau and T. Petroliagis (1995). Error growth and estimates of predictability from the ECMWF forecasting system. *Quart. J. Roy. Meteor. Soc.*, **121**, 1739–71.

Smagorinsky. J. (1963). General circulation experiments with the primitive equations. I: The basic experiment. *Mon. Weather Rev.*, **91**, 99–164.

(1969). Problems and promises of deterministic extended range forecasting. *Bull. Am. Meteorol. Soc.*, **50**, 286–311.

Straus, D. M. and F. Molteni (2004). Flow regimes, SST forcing, and climate noise: results from large GCM ensembles, *J. Climate*, **17**, 1641–56.

Straus, D. M. and J. Shukla (2000). Distinguishing between the SST- forced variability and internal variability in mid-latitudes: analysis of observations and GCM simulations. *Quart. J. Royal Meteor. Soc.*, **126**, 2323–50.

Sud, Y. C., J. Shukla and Y. Mintz (1988). Influence of land-surface roughness on atmospheric circulation and rainfall: a sensitivity study with GCM. *J. Clim. Appl. Meteorol.*, **27**, 1036–54.

Wallace, J. M., S. Tibaldi and A. J. Simmon (1983). Reduction of systematic forecast errors in the ECMWF model through the introduction of an envelope orography. *Quart. J. Roy. Meteor. Soc.*, **109**, 683–717.

Williamson, D. L. and A. Kasahara (1971). Adaptation of meteorological variables forced by updating. *J. Atmos. Sci.*, **28**, 1313–24.

Xie, P.-P. and P. A. Arkin (1996). Analyses of global monthly precipitation using gauge observations, satellite estimates, and numerical model predictions. *J. Climate*, **9**, 840–58.

Xue, Y. and J. Shukla (1993). The influence of land surface properties on Sahel climate. I: Desertification. *J. Climate*, **6**, 2232–45.

Zebiak, S. E. and M. A. Cane (1987). A model El Niño–Southern Oscillation. *Mon. Weather Rev.*, **115**, 2262–78.